Spectrum of Engineering Sciences
ISSN (e) 3007-3138 (p) 3007-312X Volume 3, Issue 10 , 2025

"Recent Developments in 2D Metal–Organic Framework Nanosheets: From Synthesis to Multifunctional Applications"

[1*]Lala Rukh Sidra, [2]Tanzeela Zulfiqar, [3]Sana Rasheed,[4]Bina hussnain,[4]Nayer Sultana, [4]Abdul Rahman, [4]Samina Kousar

[1]*Department of Chemistry, The Superior University, Lahore, Pakistan (l.r.sidra2016@gmail.com)*
[2]*Department of Environmental Sciences, Fatima Jinnah women University Rawalpindi, Pakistan (tanzeelazulfiqar18@gmail.com)*
[3]*Department of Biochemistry, Uppsala University, Sweden (sana.rasheed.2160@student.uu.se)*
[4]*Department of Biochemistry, University of Jhang, Pakistan (Munqabatzahra@gmail.com) (baharalishan651@gmail.com) (Rehman0700086@gmail.com) (saminaqaosr@gmail.com)*

DOI: https://doi.org/10.5281/zenodo.17288242

Keywords
2D Material, Metal–organic frameworks (MOFs), Composites, Nanosheets, Applications

Article History
Received on 08 Sep 2025
Accepted on 08 Sep 2025
Published on 6 Oct 2025

Corresponding Author: *
Lala Rukh Sidra

Abstract

The 2D nanosheets of metal-organic frameworks (MOFs) have surfaced lately as a promising material whose vast surface area, abundance of active sites and atomic-level thickness make them attractive in a broad range of electrocatalytic areas. To encourage the commercial applications of energy conversion and devices, efficient electro catalysts with low over potentials are greatly needed for the hydrogen evolution reaction (HER), oxygen evolution reaction (OER), and general water splitting. Due to the quick charge transfer, mass transport and increased number of surface-active sites, the special qualities resulting from the combination of 2D structure with MOF provide potential for higher electrochemical activity. In this review, we highlight the latest advancements in the study of 2D MOF nanosheets with a particular emphasis on production and applications. First, we provide an overview of the various top-down and bottom-up synthetic techniques utilized to produce 2D MOFs. The development of 2D MOF nanosheets as an electrochemical sensing platform, metal ions removal, water pollutant degradation, light emitting parts, environmental monitoring, antimicrobial activity of MOFs are further advancements.

INTRODUCTION

Since the first separation of a graphene monolayer in 2004, which led to a breakthrough in both industry and material research, two-dimensional (2D) materials have attracted a lot of scientific attention (Low, Cao et al. 2014). A vast range of innovative 2D materials, in addition to graphene have drawn significant research interest, including transition metals dichalcogenides (TMDs), hexagonal nitride of boron (h-BN),

elements such as borophene, phosphorene, silicene, germanene, antimonene and layered double hydroxides (LDHs) as well as graphite-carbon nitride (g-CN) (Mannix, Kiraly et al. 2017). One factor that is crucial in defining a material's qualities is its dimensionality (Mas-Balleste, Gomez-Navarro et al. 2011). When the contact between layers is minimal, the material has good characteristics and physical processes like charge transport are severely constrained. Due to their ultrathin atomic thickness, 2D layered materials have a variety of useful features, including great mechanical flexibility and optical transparency, which are utilized in transparent and flexible electrical devices. It is suited for use as a membrane for gas separation due to its large traverse size and because of the vast number of easily accessible active reaction sites provided by its extraordinarily high specific surface area, its catalytic activity is increased (Li, Song et al. 2013). Owing to their distinct electrical, mechanical and optical characteristics, 2D nanomaterials are extremely important in a variety of applications, including optoelectronics, sensors, energy conversion, storage and catalysis (Varsha and Nageswaran 2020, Khan 2024).

An expanding family of hybrid materials made up of organic ligands and metal containing nodes (ions or complexes) is called MOF (metal organic framework). These substances are part of a group of highly organized porous crystals that have unique properties including an extensive region of focused surface (extending above 6000 $m^2 g^{-1}$), unsaturated metal coordination site, exceptionally high porosity, programmable pore size, controllable surface characteristics and a range of morphologies (Gangu, Maddila et al. 2016). Since then, the quantity of research findings on MOF-based materials has increased at a never before seen rate within the material domain science (Wang, Kim et al. 2020). The topological diversity of MOFs crystal structures, which may be adjusted based on the study area of interest, makes them special. MOFs have the potential to be utilized to create one-dimensional (1D) nanorods, zero-dimensional (0D) nanoparticles and nanowires. Several research papers have been published on bulk three-dimensional (3D) MOF crystals and (1D) nanorods. The particular requirements for diverse applications are not totally met by bulk MOF crystals, hence 2D MOF nanosheets have recently seen a rise in research activity. Although MOF has remarkable features, its limitations such as poor chemical stability and low electrical conductivity prevent its use in the field of electrochemistry (Zhang, Yan et al. 2018, Venkateswarlu, Vallem et al. 2023).

Four varieties of MOFs may be distinguished based on their spatial dimensions: zero, one, two, and three dimensions (Qiu, Liang et al. 2020, Pan, Zhu et al. 2023) The qualities and advantages of MOFs in various applications are influenced by their size-dependent structural composition (Zhang, Liu et al. 2018). The architectures of molecular clusters and 0D MOFs are similar. They have a single molecule capacity, yet they are easy to synthesize and describe because to their basic structure. The size and form of the pores may also be precisely altered (Ahsan, He et al. 2022). 1D MOFs are typically composed of linear metal complexes. Due to a lack of continuous electron transfer pathways in the organic ligand framework, most 0D and 1D MOFs have poor charge-transfer rates, which lowers MOF activity (Zheng, Sun et al. 2022). Nonetheless, low dimensional MOFs are valuable for research in fields like electrocatalysis and sensing because of their unique geometric and electrical characteristics. Understanding patterns in the collapse, aggregation and diffusion hindrance of low-dimensional MOFs during catalysis is very important (Yang, Liang et al. 2022, Guo, Ding et al. 2023) 3D MOFs are three-dimensional spatial structures composed of metal ions and ligands. 3D MOFs often have complex structures that need complex experimental setups and technical standards. Although their pore size and shape can accommodate a greater number of molecules, they may also be challenging to control, which may affect how effectively they function in certain application areas (Hu, Yang et al. 2022, Miao, Chen et al. 2023). Apart from their excellent thermal and electrical conductivity, confinement effects, ease of

characterization and highly adjustable pore structure, 2D MOFs are a type of network material that, unlike MOFs in other dimensions, maximizes the active surface sites and charge transfer kinetics of the unique 2D structure (Zhao, Lu et al. 2022). Moreover, 2D MOFs may be composited with other materials to produce 2D MOF derivatives or composites formed from 2D pure MOFs by using the best procedures. This procedure may provide materials with higher stability and electrical conductivity while retaining the outstanding properties of the 2D pristine MOFs. (Feng, Lei et al. 2018). Current research has focused on 2D MOFs strong catalytic activity, biocompatibility, remarkable stability, durability, selectivity and separation performance (Aykanat, Meng et al. 2022). One of the main areas of research at the moment is the controlled synthesis of (2D) MOFs with well specified structures (Takenaka, Ishihara et al. 2021).

Two broad categories may be used to categorize synthetic approaches for 2D MOFs, Top-down and bottom-up strategies (Tang, Yang et al. 2020, Nivetha, Sharma et al. 2023). A few past research on the components of MOF materials linked to synthesis have been published; Zhao et al., for example, discussed the most recent advancements in materials related to 2D MOF nanosheets (Zhao, Huang et al. 2018). The logical design and growth of MOFs on MOF heterostructures and assembled several targeted MOF-on-MOF composites for graded MOFs. (Chai, Pan et al. 2021). Wang et al. provided a comprehensive overview of the methods for producing 2D MOFs and improving their performance, with a focus on identifying the catalytic mechanism and valuable active sites of 2D pure MOFs as efficient electrochemical hydrolysis electrocatalysts (Wang, Lin et al. 2023). Researchers may design the active site milieu by combining and selecting metal clusters/ions, organic ligands, functional materials, modifiers and post-processing methods (Song, Chen et al. 2021). The opportunities and challenges for the further development of materials related to 2D MOF. This will facilitate the implementation and advancement of 2D MOF related materials in the field of renewable energy by thoroughly and systematically disseminating relevant information to scholars in related fields and highlighting their unique characteristics.

1.1. The structure of nanosheets from metal organic frameworks

The basic idea underlying in order to produce 2D nanosheets, materials having weak directed interactions between layers in the bulk material must be designed with strong directed contacts inside a plane. The graphene serves as an illustration of this, since its hexagonal lattice is held together by strong covalent carbon-carbon bonds and very moderate dispersion interactions (De Andres, Ramírez et al. 2008). Throughout the MOFs layers, connection may be supplied by linked inorganic clusters, a combination of the two or organic ligands joining individual metal ions or clusters. Ionic, hydrogen bonding and dispersive interactions frequently coexist in any connection in the third dimension enabling the isolation and division of the distinct layers. Here, we group examples of MOFs that have similar ligands and structural motifs in an effort to illustrate the range of structures that have been thus far explored (Zhu and Xu 2014, Senkovska, Bon et al. 2023).

1.2. Metal Organic Framework Nanosheets based on carboxylate

The most typically used organic ligands to create MOFs are polycarboxylates similar to MOFs, because of the powerful directed coordination chemistry in them and the large variety of ligands that are offered for sale. The paddlewheel (PW) motif is the ideal secondary building unit (SBU) for creating MOFs, it is composed of two metal cations with axial ligands on top and four carboxylate ligands stacked in a plane (Fig. 1a). The traditional MOF-2 was one of the first stacked MOFs to be exfoliated to generate MOFs, it is composed of numerous layers of 1,4-benzene dicarboxylate (BDC) separated apart by Zn paddlewheels, with water molecules filling the paddlewheel's axial sites. Since then, bigger linear diacid

chains have been joined with a variety of metal ions (Cu, zn, Co), To produce isostructural MOFs, 1,4-benzene dicarboxylate and 1,3-benzene dicarboxylate derivatives were synthesized (Wang, Chi et al. 2017, Huang, Li et al. 2018).

To minimize interlayer connections and encourage exfoliation into solvent, the 1,4-benzene dicarboxylate has been functionalized with chains of weakly interconnecting alkyl ethers (Fig. 1c). Many MOFs based on the tetrakis(4-carboxy-phenyl)porphyrin (TCPP) structure have been successfully synthesized in combination with a variety of metal-PWs (Zn, Cu, Cd and Co) (Fig. 1d) (Makiura, Motoyama et al. 2010). Through the use of distinct metal ions connected to the porphyrin and PW sites, this motif also makes it possible to produce bimetallic MOFs. Due to their high degree of connectivity and preorganization, porphyrin units are perfectly suited for the creation of MOFs (Ashworth and Foster 2018, Wang, Zhang et al. 2023).

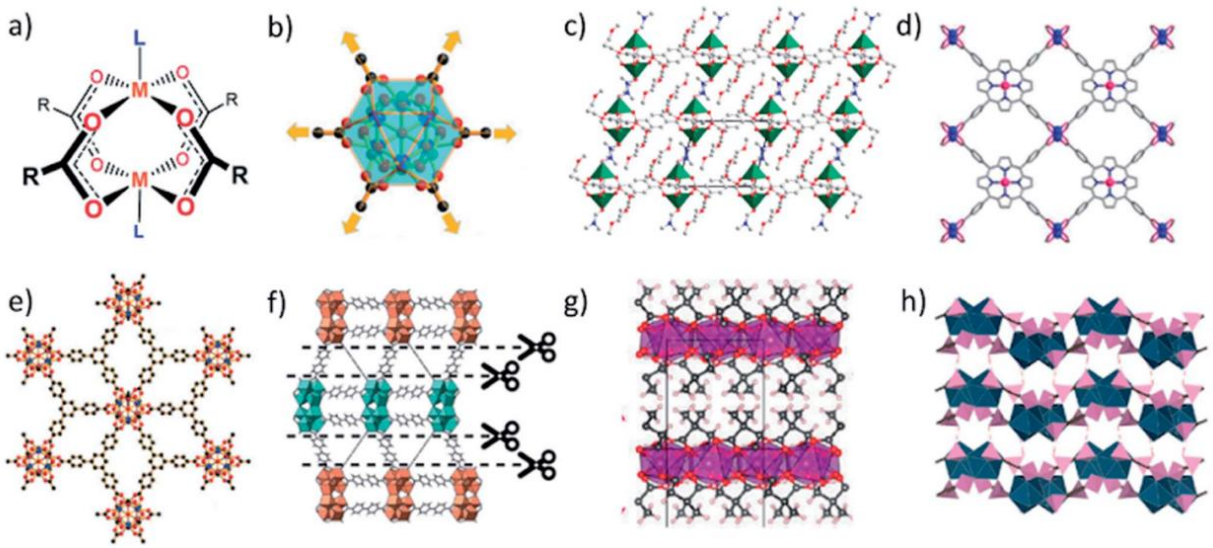

Figure: 1. Schemes illustrating the paddlewheel and M_6L_6 secondary construction units, respectively. Examples of crystal structures (from c to h) that show the various secondary building blocks and carboxylic acid-based linkers used to create MOFs Specifically ;(c) $Zn_2(BDC\text{-}x_2)(DMF)_2$, in which x ¼ $O(CH_2)_3OMe$; (d) M(TCPP) where M ¼ zinc, copper, cadmium, Co; (e) [Hf_6 (m_3-O)$_4$(m_3-OH)$_4$(carboxylate)$_{12}$]; (f) hcp UiO-67; (g) Mn(DMS)(H_2O); (h) lanthanum 1,3,5-benzenetriphosphonate (LBP-II). (Tan, Saines et al. 2012, Araki, Kondo et al. 2013, Foster, Henke et al. 2016, Wang, Zhao et al. 2016, Cliffe, Castillo-Martínez et al. 2017, Chang, Chen et al. 2021).

Zr and Hf carboxylate cluster have been successfully used as SBUs (secondary building unit) to construct robust 3D MOFs, while 2D MOFs have just recently been produced utilizing these SBUs. Benzoene 1,3,5-tribenzoate (BTB) moieties were linked with 3-connected carboxylate ligands to generate an infinite 3,6-connected 2D system with kagome double (kgd) topology using the Hf^{4+} cluster [Hf_6(m_3-O)$_4$(m_3-OH)$_4$(carboxylate)$_{12}$] (Fig. 1e). Because the Hf_6 cluster's connectivity does not match the geometric criteria of a 2D layer, they employed format to cover six of the cluster's connection points while retaining the other six in the same plane for BTB ligand interactions (Fig. 1b). The Hf and Zr $M_6O_4(OH)_4$ clusters that were produced by controlled hydrothermal synthesis to construct similar layered structures based on BTB (Zhao, Zuo et al. 2021) and recently presented a continuous flow manufacturing technique the Zr

counterpart (Wang, Li et al. 2018). With distinct sites closed, the Zr_6 cluster was utilized to create MOFs using tetracarboxylate based on tetraphenylethylene (TCBPE) and TCPP ligands. They were able to produce a pair of clusters ($Hf_{12}O_8(OH)_{14}$) with a Hf_{12} cluster, which they were able to exfoliate by carefully selecting which interlayer ligands to scission (Fig. 1f). An SBU with extended tritopic carboxylates has also been employed with a double-decker Hf_{12} clusters that is comparable to this one (Cliffe, Castillo-Martínez et al. 2017). Additionally, coordination bonding (O) and 2D layers are created using inorganic (I) corner-sharing octahedral. Nomenclature uses superscript numbers to denote the various types of connections in the various dimensions. They built a number of layered frameworks out of 2,2-dimethylsuccinate (DMS) and its isomers as well as other metal ions and then exfoliated them to form nanosheets (Nath, Chakroborty et al. 2023)). The standard Mn-DMS network may be shown in Fig. 1g. Deformed MnO_6 octahedral creates corner-sharing chains along the b-axis, which are linked by DMS ligands to form 2D layers. The methyl groups of the ligands that extend between the layers form the weakly interacting hydrophobic caps. Similar systems in other cases displayed two-dimensional organic (I^0 O^2) or inorganic (I^2 O^0) connectivity, highlighting the challenges of structure prediction with fewer pre-organized ligands. Inorganic layers can likewise be produced using the phosphonic acids. Coupling 1,3,5-benzene triphosphonate to lanthanum ions to generate multilayer MOFs may be advantageous because to the high coordination values of lanthanide ions (I^1 O^1) or (I^2 O^0) connectivity (Fig. 1h) (Ashworth and Foster 2018).

1.3. Coordination nanosheets based on N-donors

The impartial N-donor framework 4,4-bipyridine (bpy) was used to construct $Cu(bpyh(OTf)_2)$ and the trifluoromethanesulfonate (OTf) counter ions were only weakly bound at the interaction layers. Atomic force microscopy (AFM) and transmission electron microscopy (TEM) identified the single and nanoscrolls by crumpling and rolling a few layers of nanosheets. This illustrates the system's degree of flexibility, it has also been possible to use triand hexadentate terpyridine (tpy) building blocks to create self-assembling monolayers at surfaces by coordinating to different metal ions (Kuai, Li et al. 2019). Due to their multidentate binding, these multidentate construction pieces show a high level of interconnectedness and potent coordinating interactions. Interfacial construction yields mechanically robust single layered nanosheets with lateral diameters up to several cm (Wang, Wang et al. 2014). The level of crystallinity is most likely minimal by employing cooperation between ligands that are tri or tetradipyrinato and tetrahedral zinc ions, a family of coordination nanosheets with a similar structural makeup has also been created (Sakamoto, Hoshiko et al. 2015, Mustafar, Yusuf et al. 2023).

1.4. Nanosheets of coordination made of dithiolene

Due to their exceptional electrical characteristics, there has been a lot of interest in a variety of coordination nanosheets composed of square-planar metal ions and aromatic bis(dithiolenes). For instance, benzenehexathiol (BHT) and d^8 metal ions Ni(II) and Pd(II) are examples, collaborated to produce Ni(II) bis(dithiolene) motif-containing planar nanosheets with a six-fold symmetry (Dong, Pfeffermann et al. 2015). Through the phenylene linker, these complexes show significant charge delocalization in mixed valent states among the three metalladithiolene units. Apart from the amino analogues, extended iterations of these systems have been generated by the use of triphenylene hexathiolate with nickel present and cobalt (Abhervé, Mroweh et al. 2021). At the surface of acetylacetonate, hexaminobenzene and metal ions including Ni^{2+}, Cu^{2+} and Co^{2+} interacted to produce thin sheets that were a few microns wide and moderately conductive. These materials individual sheets haven't been divided, but hexaminotriphenylene has been reacted with Ni and Cu ions to create longer versions of these layered materials, which are used to create semi-conductive frameworks (Chen, Dai et al.

2015). Hexaminotriphenylene and triphenylene hexathiolate have also been combined with Ni^{2+} or Co^{2+} ions to create mixed amine/thiolene coordination nanosheets with comparable structures (Sun, Wu et al. 2017).

Due to their exceptional electrical characteristics, A class of MOFs containing aromatic bis(dithiolenes) and square planar metal ions has piqued the curiosity of researchers. For example, when d^8 metal ions and benzenehexathiol (BHT) interacted to form 2D planar nanosheets with six fold symmetry, such as Pd(II) and Ni(II), the nickel bis(dithiolene) motif was formed. In mixed valent states, these complexes show notable charge delocalization between the three metalladithiolene components via the phenylene linker. These systems have been expanded by combining nickel, cobalt and triphenylene hexathiolate. The amino equivalents of these substances have also been studied. By treating hexaminotriphenylene with Ni and Cu ions, expanded equivalents of these layered materials were formed; nevertheless, the constituent portions of these materials have not yet been separated. The hexaminobenzene reacts with Ni^{2+},Cu^{2+} and Co^{2+} acetylacetonate at an interface, it is around 10 nm thick and many microns wide and it has been demonstrated that this interface is weakly conducting (Sun, Wu et al. 2017). Pairings of hexaminotriphenylene, Ni or Co and Ni(1,3,5-triaminobenzene-2,4,6-trithiol) with triphenylene hexathiolate have also been used to produce mixed amine/thiolene MOFs with comparable structures (Ashworth and Foster 2018, Mustafar, Yusuf et al. 2023).

1.5. $Ni(OH)_2$ nanosheets

The monolayer $Ni(OH)_2$ nanosheet in Ni-MOF functioned as a precursor to the Ni species. The nanosheets were created by following previous studies (Ida, Shiga et al. 2008). For a full procedure, refer to the supporting documentation. Monolayer nickel hydroxide nanosheets with a thickness of 1 nm were created by exfoliating layered nickel hydroxide in formamide (1mg solid in 1mL solvent). Using AFM, HR-TEM and SAED, the thickness of the monolayer and other characteristics were verified. In order to make 2D Ni-MOF, a 10 mL DMF/water (7:3) solution containing 0.13 mmol of 1,4-benzenedicarboxylic acid (BDC) and a 10 mL DMF dispersion containing 0.16 mmol $Ni(OH)_2$ monolayer nanosheet were combined. This resulted in Ni-BDC-MOF, also known as Ni-BDC-MOF. After that, the mixture was heated for 0.5–12 hours at 90 °C while being sealed tightly (described in the Supporting Information). The finished product was characterized using field emission scanning electron microscopy (FE-SEM), powder Xray (PXRD), thermogravimetric (TG) investigations, SAED, AFM, HR-TEM and SAED. The MOFs acquired via this approach will now be addressed as P-NiMOF-t-T (where P-NiMOF stands for powder species obtained using solution method, t for time, and T for reaction temperature) (Ida, Shiga et al. 2008) and the PXRD pattern of P-NiMOF-12-90 match (Figure 2a). Under FE-SEM, P-NiMOF 12-90 displayed a uniform, rectangular sheet-like shape (Figure 2b). SAED provided further confirmation of its crystal structure (from HR-TEM). SAED perfectly matches the expected pattern produced by the Ni-BDC-MOF (010) miller plane (Figure 2c,d) (Pathak, Hatakeyama et al. 2023).

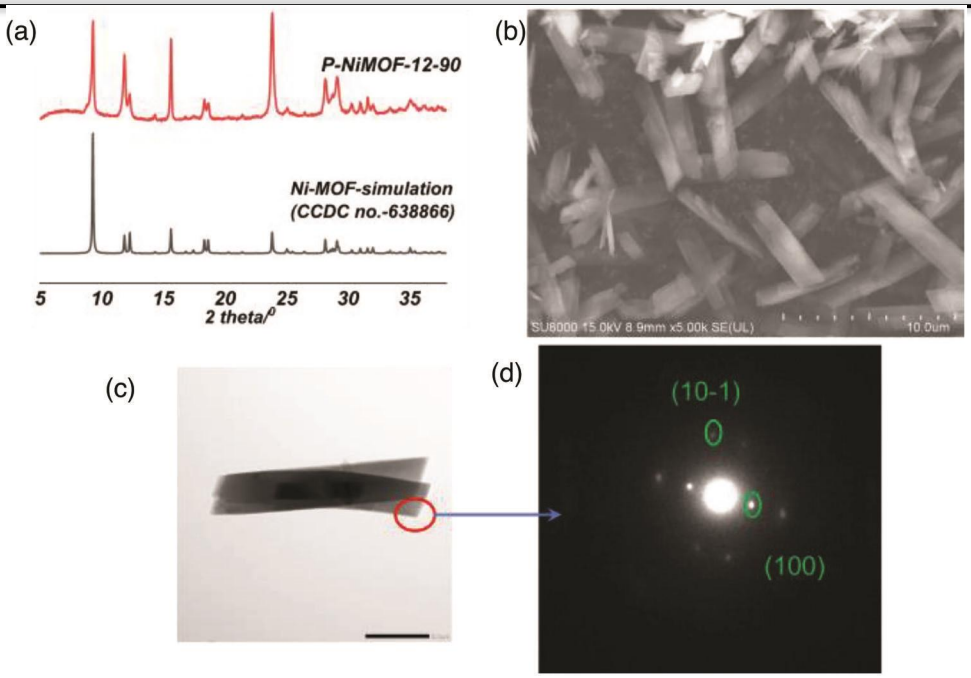

Figure 2. a) PXRD patterns of 2D-Ni-MOF (red line), synthesised P-NiMOF-12-90, and simulated PXRD pattern (black line). The images of P-NiMOF-12-90 are as follows: b) FE-SEM picture, c) HR-TEM image, and d) selected area electron diffraction (SAED) of P-NiMOF-12-90, 2D Ni-MOF (Pathak, Hatakeyama et al. 2023).

2. Techniques for producing of 2D MOF nanosheets

The thorough evaluation of trustworthy methods for creating ultrathin 2D MOF nanosheets has significant implications for in-depth research into their intriguing characteristics and prospective applications. There has been a lot of focus on the creation of efficient synthesis methods up to this point. Surfactant assisted synthesis, interfacial synthesis, three layer synthesis, competitive coordination technique and sonication exfoliation are some of these approaches (Zhao, Peng et al. 2018).

2.1. Exfoliated nanosheet preparation

Top-down techniques (such as sonication, ball milling and so on) may easily produce 2D MOF nanosheets, but because of their low elastic modulus noted earlier and huge sections of them will quickly fragment (Hermosa, Horrocks et al. 2015). The resulting membranes separation selectivity would be lowered by the irregular alignment of the 2D MOFs and the nanosheets in the membrane layer. MAMS-1 (Mesh Adjustable Molecular Sieve) crystals were here transformed into two-dimensional nanosheets using a gentle exfoliation technique based on the solvent freeze-thaw process (Fig. 3a). It is customary to spread out MAMS-1 crystals in hexane, freeze them in a liquid nitrogen bath and then defrost them in a hot water bath heated to 80°C. The recent thermal expansion-driven gas exfoliation of bulk h-boron nitride was carried out by taking advantage of the curling and expansion caused by the extreme temperature difference. According to this theory, MAMS-1 crystals kept in repeated freeze-thaw cycles would exfoliate into separate nanosheets as a result of hexane's volume-dependent shift between liquid and solid phases and the shear force produced by solid phases. It seems that MAMS-1 crystals were successfully exfoliated into bilayered MAMS-1 nanosheets since AFM found a thickness of around 4 nm in more than 95% of the locations examined. Exfoliated MAMS-1 nanosheets are required to be further purified because of their very wide lateral size distribution (4.7-24.3 mm, average 10.7-4.8 mm, Fig. 3b), which may render

them unsuitable for membrane production. Following exfoliation, the MAMS-1 nanosheets exhibit a greater specific surface area of Brunauer-Emmett-Teller (BET) compared to bulk crystals (24.8 m^2 g^{-1} to 126.1 m^2 g^{-1}; Fig. 3c). This provides further proof that the exfoliation procedure is successful. Specifically, compared to the bulk crystals, the exfoliated nanosheets external surface area (Sext) increases by a factor of six. Exfoliation increases the micropore surface area and partly opens the bulk crystal micropores in the interim. The crystal planes of the substance's (420) unit cell are commensurate with the lattice spacing of the exfoliated MAMS-1 nanosheets, which is 0.24 nm, based on TEM images of the materials (Fig. 3d).

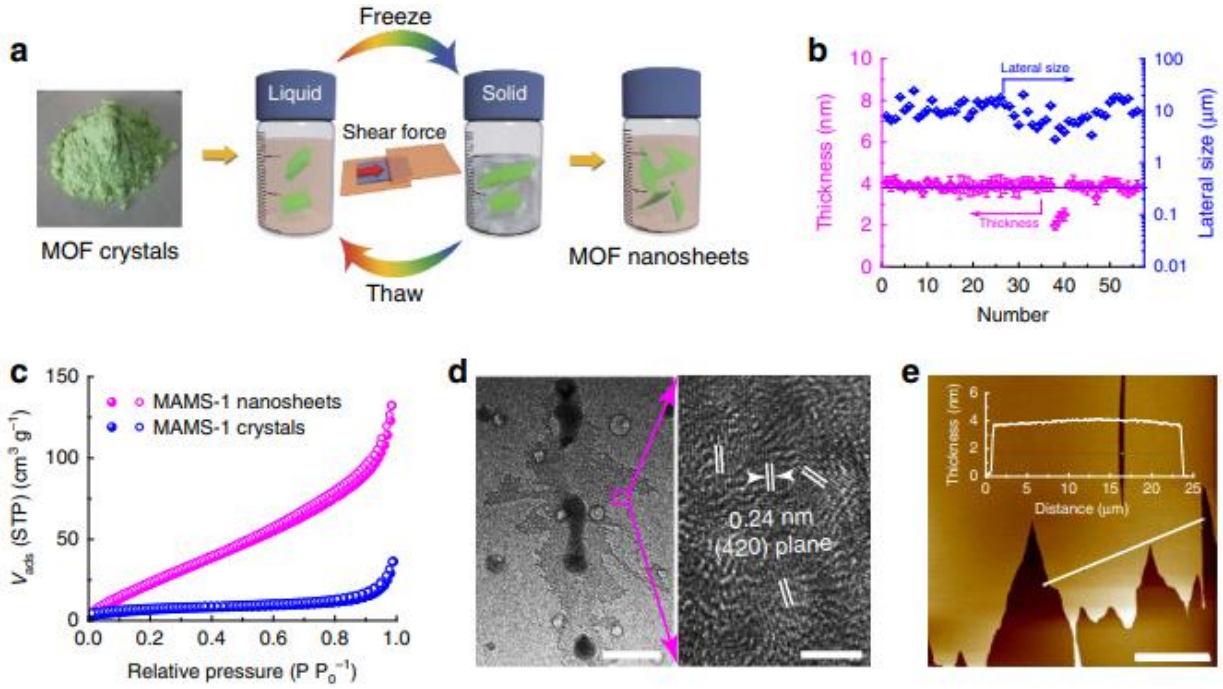

Figure: 3. MAMS-1 nanosheet exfoliation and purification. (a) During freeze-thaw cycles, the MAMS-1 crystals split apart to form scattered nanosheets. (b) Exfoliated MAMS-1 nanosheets' thicknesses and lateral distribution of their sizes are shown, following a 10-cycle freeze-thaw in hexane. A bilayered MAMS-1 nanosheet's optimal thickness is shown by the horizontal line. (c) N_2 sorption isotherms of MAMS-1 that has crystallized and that has been exfoliated (packed for adsorption and open for desorption) at 77 K. A TEM image of nanosheets from MAMS-1. 1 mm (left) and 3 nm (right) scale bars. (e) MAMS-1 nanosheets following purification as seen in an AFM image. Scale bar of 10 mm (Wang, Chi et al. 2017)

MAMS-1 bulk crystals and exfoliated nanosheets Fourier transform infrared (FTIR) spectra are identical, demonstrating that the chemical structure of MAMS-1 was preserved throughout exfoliation (Hermosa, Horrocks et al. 2015, Lin, Li et al. 2024). Up to 300 ^{0}C, thermal stability of the exfoliated MAMS-1 nanosheets is almost equal to that of bulk crystals, allowing for use in high temperature applications. The findings suggest that successful exfoliation of bulk MAMS-1 crystals into discrete MAMS-1 nanosheets with high aspect ratios is a critical step towards the fabrication of nm-thick two-dimensional molecular sieving membranes (2,8001,200, calculated by the data in Fig. 3b).

2.2. Both bottom-up and top-down synthesis

2D growth is favored during an detained crystallization, which is comparable to the "bottom-up" synthesis of MOFs. By using ligands and SBUs that preferentially crystallize in two dimensions, it may be possible to create nanosheets without further modifying them. To create Cu(TCPP) MOFs with 33 layers and with DMF and EtOH, a solvothermal synthesis (3: 1 v/v), an average thickness of 15 nm was achieved (Fig. 5a) (Kitagawa, Dokko et al. 2005). By adhering to the surface of the expanding nanosheets, surfactants can alter crystal habit by limiting development and layer stacking. Two-dimensional growth is favored during an arrested crystallization, which is comparable to the "bottom-up" synthesis of MOFs. By using ligands and SBUs that preferentially crystallize in two dimensions, it may be possible to create nanosheets without further modifying them.

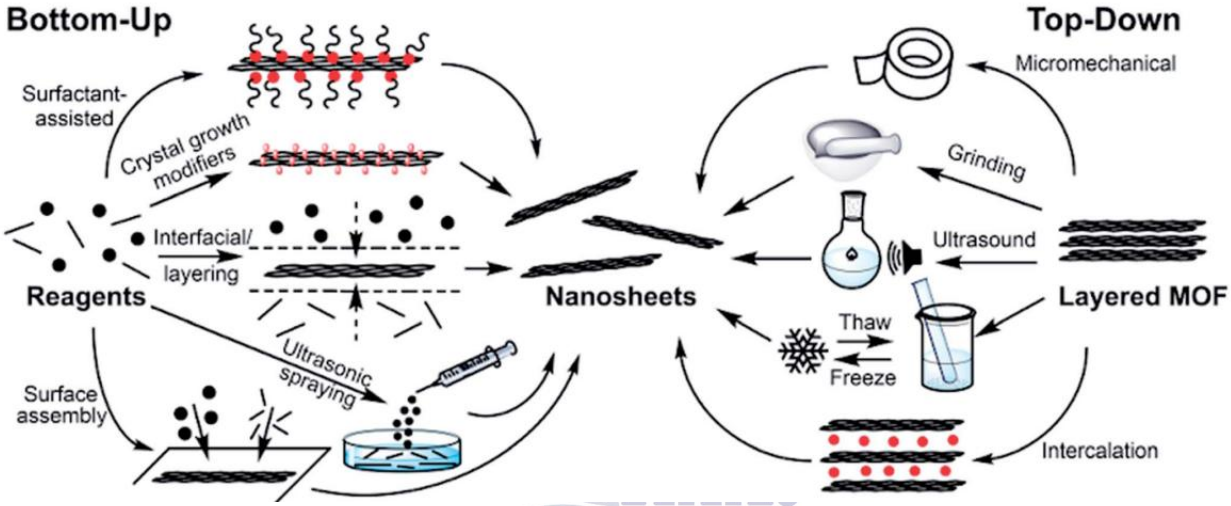

Figure: 4. Schematic illustrating several top-down and bottom-up methods used to create MOFs. (Ashworth and Foster 2018)

Following the synthesis of Cu/Co/Cd(TCPP), which demonstrated the method's flexibility by yielding nanosheets of less than 10 nm thickness for all save Co(TCPP), these MOFs were employed for a number of uses (Cao, Zhao et al. 2016). Additionally, PVP (Polyvinylpyrrolidone) was used to create nanosheets between 30 and 55 nm thick at room temperature during the production of Cu(HBTC) (Copper(II) 1,3,5-benzenetricarboxylate) and pressure. It has been proposed that certain crystal planes can absorb the cationic surfactant CTAB (Cetyltrimethylammonium bromide). The stability and dispersion of MOF in specific solvents may be aided by the hydrophobic tail adhering to the crystal surface. Direct production of Zn(bim)(OAc) MOFs with a thickness of 7 nm has been accomplished using this method (Xue, Ma et al. 2024).

Table: 1. different 2D materials top-down and bottom-up synthesis

2D MOF	Synthesis Method	Synthesis Strategy	Topography	Thickness	Ref.
$[Cu_2Br(IN)_2]n$	Top-down Synthesis	Ultrasonic exfoliation	Uniform	0.5 ± 0.015 nm	(Amo-Ochoa, Welte et al. 2010, Ren and Xu 2024)
ZSB-1	Top-down Synthesis	Wet sphere milling/ultrasonic	Uniform	11.8 ± 2.3 nm	(Tamuly, Sama et al. 2022)

$Zn_2(bim)_3$	Top-down Synthesis	Wet sphere milling/ultrasonic	Uneven	1.6 nm	(Peng, Li et al. 2017)
Zn_2(PdTCPP)	Top-down Synthesis	Intercalation and chemical exfoliation	Uneven	1.0 nm	(Ding, Chen et al. 2017)
[Co(Ni-H7TPPP)$_2$]·8H_2O	Top-down Synthesis	Chemical exfoliation	Uneven	3.9 ± 0.2 nm	(Qin, Mu et al. 2021)
$Co_6O(dhbdc)_2$	Top-down Synthesis	Electrochemical/chemical exfoliation	Wrinkled	2 nm	(Huang, Li et al. 2018)
ZIF-L	Bottom-up Synthesis	Template assisted	Uneven	5.5 μm	(Li, Hou et al. 2019)
Meso-CuBDC	Bottom-up Synthesis	Sacrificial templates	small square shape	8.0 nm	(Wang, Wang et al. 2020)
Ag_3BHT_2	Bottom-up Synthesis	liquid–liquid interfacial growth	Disordered	200 nm	(Chen, Lu et al. 2018)
Ni-MOF	Bottom-up Synthesis	liquid–liquid interfacial growth	Uniform	5 nm	(Wang, Dong et al. 2021)
CuBDC	Bottom-up Synthesis	Interfacial synthesis	Uniform	5–25 nm	(Rodenas, Luz et al. 2015)
Zn-TCPP	Bottom-up Synthesis	Surface-active agent-assisted	Uniform	7.6 ± 2.6 nm	(Zhao, Wang et al. 2015, Li, Yoshida et al. 2024)
Co/Zn-porphyrin	Bottom-up Synthesis	Surfactant-assisted	Wrinkled	4–5 nm	(Ma, Bai et al. 2022)
HXP	Bottom-up Synthesis	Molecular modulation assisted	Uniform	20 nm	(Lin, Wan et al. 2020)
[Cu(2,5-pydc)(H_2O)]$_n$·2H_2O	Bottom-up Synthesis	Ultrasonic exfoliation	Uniform	126 nm	(Contreras-Pereda, Moghzi et al. 2021)
Ni_3S_2@2D Co-MOF	Bottom-up Synthesis	Self-sacrificial template	Rough	60 nm	(Cheng, Yang et al. 2022)
NiCoSe	Bottom-up Synthesis	ion-exchange	Uniform	230 nm	(Zhou, Chen et al. 2021, Li, Zhou et al. 2024)

Small molecule crystal growth regulators that selectively attach to a certain crystal's facet can change the crystal habit that results. One well known instance of this is the creation of massive nanosheets up to 500 nm^2 when pyridine was introduced while the pillared MOF was being synthesized [Cu_2(NDC)$_2$ (DABCO)] (where NDC is 1,4-naphthalene dicarboxylate and DABCO is 1,4-diazabicyclo [2.2.2] octane). PVP has been used to produce Co(TCPP)(BiPY) pillared MOF highly anisotropic nanosheets with a comparable result. Note that these nanosheets do not fit our concept of a MOF since they are joined in three dimensions by coordination bonds. To make single layers or pillared bilayers. However, with two-dimensional connectivity, this method might theoretically be applied (Cao, Zhao et al. 2016).

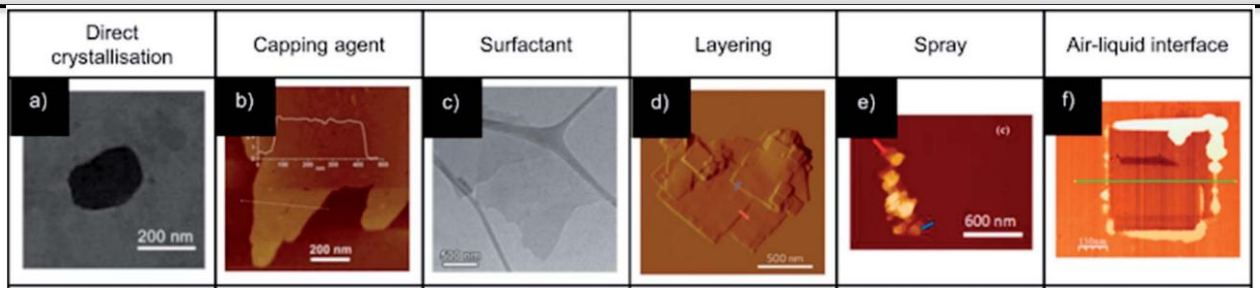

Figure: 5. Examples of AFM (b, d) and TEM (a, c) pictures showing different top-down (g^{-1}) and bottom-up (a-f) methods used to create MOFs. According to the provided vectors, the nanosheets predicted heights are as follows: (b) - 3 nm; (d) - 6 and 8 nm (red and blue, respectively); (e) both 5 nm; and (f) - 0.8 nm, respectively (Bauer, Zheng et al. 2011, Xu, Yamada et al. 2012, Rodenas, Luz et al. 2015, Zhao, Wang et al. 2015, Hu, Mahdi et al. 2017, Li, Wang et al. 2017)

The incorporation of small molecules into developing MOFs can also lead to the development of multilayer structures. Acetic acid can be used as a modulator to stop networks from joining. This resulted in the creation of MOFs with a thickness of 10–20 nm that are more stable than corresponding 3D MOFs (Fig. 5b) (Hu, Mahdi et al. 2017). When six format ions are added to Zr_6 and Hf_6 SBUs, their 12-connectivity may vary, resulting in the development of 10 mm-thick nanosheets that are observable down to monolayer thickness.

To function as a modulator, tiny monoacid ligands (formic, acetic, lauric and oleic acid) were introduced to the reaction mixture at precisely calibrated quantities. This resulted in layered MOFs where the monoacids took up residence at the Zr cluster's interlayer coordination sites, leading to the destabilization and "disassembly" of MOFs (as confirmed by quantitative NMR and SAXRD). Under TEM, the generated MOFs stacked and the aliphatic chain lengthened. To build a series of nanosheets with a maximum square size of 4 mm and a thickness of 5-25 nm using the "layered synthesis" method (Fig. 5c), By dissolving the ligands and metal ions in different ratios of DMF to acetonitrile, different densities of solutions were created. These solutions were then piled one on top of the other, with a buffer layer in between. As a result of the delayed diffusion of the ligand and metal ions into the buffer layer, nanosheets developed preferentially in two dimensions. The subsequent gravitational sinking of these nanosheets into a layer devoid of metal ions prevented further development (Fig. 5d). Inspired by this research a spray approach applied a metal salt solution to a reservoir of ligand solution using ultrasonic atomization. By minimizing the disruption brought on by layer contact, this method creates a stable interface for anisotropic crystal formation. This technique resulted in 5 nm-thick nanosheets (Fig. 5e).

Utilizing phase interfaces, such the air-liquid interface (Fig. 5f, for instance) or liquid-liquid interfaces is another method for regulating the growth of crystals in two dimensions (Tsukamoto, Takada et al. 2017, Menamparambath 2024). These methods frequently function in a natural setting. To produce liquid gas interfacial growth, Langmuir-Blodgett troughs were utilized, which apply a ligand solution in a volatile solvent on top of an aqueous phase containing metal ions (Motoyama, Makiura et al. 2011). Although the crystallinity of these massive sheets is being questioned, surface compression can yield huge extended nanosheets with domains as tiny as sub-mm. These massive MOFs may also be deposited one layer at a time to create MOF films. In a recent, more comprehensive technique and examples of nanosheets created in these manner are presented (Rubio-Giménez, Galbiati et al. 2018). There have been several examples of how MOF layers have grown at solid-liquid interfaces. We won't go into depth about these methods here because they have recently been evaluated elsewhere and because it

is tough to remove them from the surfaces (Rubio-Giménez, Galbiati et al. 2018). Even though the bulk of MOFs are not intrinsically two-dimensional, growing MOFs atop other materials with two dimensions such as graphene oxide is an attractive process that has been investigated (Li, Yang et al. 2016, Naser, Badmus et al. 2023).

2.3. Materials in two dimensions with unique and distinctive structural characteristics

Numerous materials with two dimensions with fascinating and unique structural characteristics exist. However, their thorough examination of membrane based separation is absent. Despite major advances in the creation of two-dimensional material based membranes, as demonstrated in Table 2, there are still difficulties that need to be solved before they can be used in practical applications.

2.4. Structure and Characteristics

Because of its low dimensionality, 2D MOF nanosheets have special physical and chemical characteristics. Moreover, by modifying the metal nodes or organic ligands, a variety of compositions and behaviors may be achieved, offering benefits for certain applications. This section will examine, using certain applications, how the 2D MOF structure affects its performance (Lee, Shokouhimehr et al. 2022). One easy efficient and versatile way to prepare for creating porous structures is using ice stenciling. The capacity of Ice crystals are cryogenically frozen in situ because they reject compound particles. In the end, the cooling rate and solution concentration govern these interactions (Zhang and Cooper 2007). Song et al. used the ice template method to self-assemble quasi-ordered ZIF-8 nanoparticle alignment, which produced 2D superstructures. Crystallographic planes were used to align neighboring polyhedral MOF particles. (Figure 6a). The aqueous ZIF-8 nanoparticle solution was rapidly frozen in liquid nitrogen and then the ZIF-8 self-assembled 2D superstructures were produced by freeze-drying. Truncated rhombic dodecahedral and cubic MOF nanoparticles may create a range of self-assembled structures, such as the monolayer TRZ8-1/Cub-Z8-1 and the bilayer TRZ8-2/Cub-Z8-2 structure, by varying the concentration. The volume-increasing ice during the freezing phase repels ZIF-8 NPs into the liquid phase, resulting in the formation of colloids. The ZIF-8 particle concentration is much greater in the channels between adjacent ice crystals where these colloids are pushed by a pressure differential. As the ice passes through the system, its narrowing channels enclose the ZIF-8 NPs, where their concentration rises. When the final condition of freezing is reached, the size of the channel, which is confined within the gaps between the metal MOF particles, is comparable to that of the ZIF-8 particles (Song, Song et al. 2022).

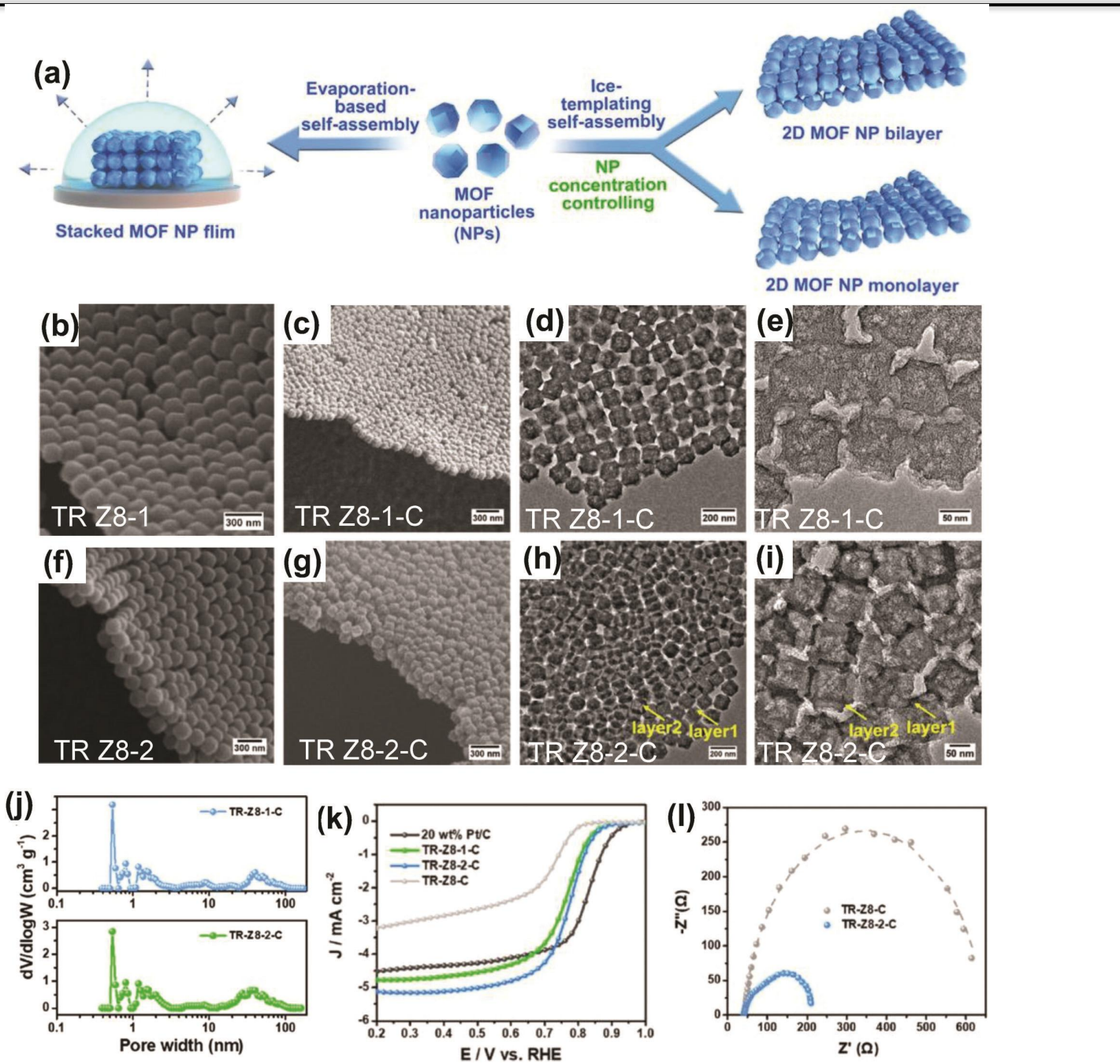

Figure: 6. Making carbides and high-performing 2D ZIF-8 MOF using an ice template. Schematics showing the two ways MOF superstructures may be constructed. b) The monolayer SEM picture of TR-Z8-1. c) SEM image TR-Z8-1-C; d, e) TEM images. f) Bilayer SEM image of TR-Z8-2. g) SEM (TR-Z8-2-C) and h,i) TEM images. j) The TR-Z8-1-C and TR-Z8-2-C pore size distribution NLDFT plots. k) LSV curves in 0.1 m O_2-saturated KOH for 20 weight percent Pt/C, TR-Z8-C, TR-Z8-1-C, and TR-Z8-2-C (rotation rate: 1600 rpm; sweep rate: 2 mV s^{-1}). l) Nyquist plots for TR-Z8-C and TR-Z8-2-C, obtained at 0.7 V (against RHE) (Song, Song et al. 2022).

Table: 2 Different MOF materials and their properties

2D materials	Membrane separation	Structural properties	Synthesis methods	Reference
MOFs	MOF membranes that are clean and have high H_2/CO_2 selectivities. Exceptional performance in the separation of CO_2 and N_2. High CO_2 sorption affinities and olefin-based gases as well as an anti-plasticization function are promising characteristics for fillers used in the manufacture of MMMs. It is difficult to produce pure MOF-based membrane on a large scale.	Microporous structure and size selection. High CO_2 sorption capability; good polymer matrix compatibility. In comparison to GO, it has poor mechanical and chemical stability.	Bottom-up strategies Procedures for ball milling and freeze-thaw exfoliation (not yet flexible and scalable)	(Zhao, Huang et al. 2018) (Moghadam and Park 2018)
GO	Promising molecular-sieving characteristics for H_2 and CO_2 highly desired as a filler for the manufacture of MMMs anti-plasticization function. To produce vast quantities of clean GO membranes, scalable methods are necessary. The way GO flakes are stacked affects the pure GO membranes ability to transport gas.	High mechanical toughness elevated aspect ratio. Oxygen-based functions provide surfaces a rich surface chemistry.	Scalable and well-developed oxidation-assisted exfoliation manufacturing processes have a limited capacity to disperse in organic solvents.	(Cheng, Datta et al. 2022)
LDHs	Because of the small interlayer spacing (0.31 nm), there is strong H_2 permeance and H_2/gas selectivity. More research on membrane-based gas separation is needed.	Functional diversity and compositional adaptability strong electrostatic interactions between layers interlayer space with high uniformity	Bottom-up approaches Liquid exfoliation helped by anion exchange (expensive cost and low manufacturing yield)	(Cardoso 2019, Kumar 2019)
h-BN	Restricted to theoretical research additional research in the area of gas separation is required.	Strong mechanical properties more reliable interlayer integrity when compared to GO Because B-N bonds are somewhat ionic,	Exfoliation of liquids using surfactant solutions and organic solvents (poor yield)	(Li, Kuppler et al. 2009, Sainsbury, Satti et al. 2012)

		functionalization is simple.		
TMDs	In comparison to GO and MOF-based membranes, MoS_2 laminate membranes demonstrated stronger H_2 permeance. Used in MMMs as filler preventing plasticization a bad fit with the polymer matrix	High mechanical toughness superior stability to GO in aqueous solutions high levels of smoothness	Surfactant solution, liquid exfoliation, and ion intercalation in organic solvents (very poor yield)	(Moghadam and Park 2019, Hu, Clark et al. 2022)

3.D layered MOF Applications.

The 2D layered MOF nanosheets have diverse properties and are used in a variety of applications due to the unique features of the two-dimensional nanostructure and MOF. In electrochemistry, MOFs are extensively utilized for sensing, energy conversion and catalysis. Electrochemical applications are aided by a large specific surface area, a flexible structure, a porous system, accessible metal active sites and a simple mass transport channel. However, the utility of certain electrolytes as an electrode material is restricted due to their poor stability and low electrical conductivity. There has recently been a lot of interest in developing innovative nanostructured 2D layered MOFs with hierarchical porosity properties (Ghosh, Fathima Thanutty Kallungal et al. 2023).

3.1. Electrochemical Sensing

The development of novel 2D nanostructured layered MOF materials for the manufacture of electrochemical sensors is a growing research area. The 2D MOF nanosheet has the potential to be used as a sensing platform due to its intriguing properties. The nanosheets have a great affinity for analytes because of their extreme thinness and substantial specific surface area (Ghosh, Fathima Thanutty Kallungal et al. 2023). By changing the predecessors, its structure may be changed, providing versatile characteristics suitable for a range of applications. Electrochemically active 2D MOFs can also be synthesized using redox active metal nodes or organic ligands. A new electrochemical sensing platform for H_2O_2 detection has been developed employing a series of 2D bimetallic MOF nanosheets having the symbol M-TCPP(Fe) (M = Co, Zn and Cu) (Wang, Zhao et al. 2016). On glassy carbon electrodes, the Langmuir-Schafer process was utilized to generate thin films of Co-TCPP(Fe) nanosheet. Among the numerous changed electrodes $(Co\text{-}TCPP(Fe))_5/GC$ demonstrated the best detection by catalytic activity of H_2O_2 with a sensitivity of 4A cm^2 mM^{-1} and a detection limit of 0.15 106 M (Yang, Chen et al. 2019). In addition, the sensor material displays a linear rise in reduction current throughout a concentration range of 0.4 106 to 50 106 M, high stability and outstanding reproducibility. Additionally, the proposed sensor was utilized to measure H_2O_2 emitted by living cells in real time, which is helpful for the early identification of breast cancer (Wang, Zhao et al. 2016, Zhong, Zhang et al. 2023).

An example of this is a 2D composite material that is used as an electrochemical aptasensor for the detection of cocaine and is made of gold (Au) nanoclusters embedded in zirconium-based MOF nanosheets. The Zr-based MOF shows strong attraction for the phosphoric group via the formation of Zr-O-P bonds. The composite is also a highly interesting sensing platform with notable electrochemical activity and considerable bioaffinity for analysis because of the enormous specific surface area of 2D nanosheets and the better electrochemical activity of Au NCs. Aptamer strands included in the modified electrode bind to cocaine exclusively. With a broad linear detection range of 0.44 pg ml^{-1}, high selectivity, and a detection limit of 0.44 pg ml^{-1}, the recommended sensor (Su, Zhang et al. 2017).

The top-down modulation method was used to create a novel porphyrin-based small crystal of MOF, 2D Zn-TCPP MOF nano-disk, with BPDC (4,4-biphenyl dicarboxylic acid) serving as the modulator. The Zn-TCPP complex's original 4-coordinate structure changes to a 5-coordinate structure when nitrite (a donor molecule) is present because of nitrite's particular affinity to MOF's axial ligand. An FTO substrate was coated with a Zn-TCPP(BP) nano-disk, which was used for nitrite detection and electro-catalytic oxidation. The updated electrode has a high sensitivity of 158.1 μA mM^{-1} cm^{-2} or 158.1 amps per millimole per square centimetre, due to the porphyrin's independent distribution across the framework. As a result, there are more nitrite ion active sites. The low detection limit of 0.26 M may have been caused by the sandwich structure of the nano-disk and the tiny size of the crystals, which allowed for a vast area of contact between the material and the nitrite ions. Furthermore, the accuracy of real-time nitrite detection in a variety of water samples ranges from 93% to 109% with appropriate recovery (Zou, Tian et al. 2020).

A glucose sensor that is not enzymatic was built using nanosheets, bimetallic Co/Ni MOF nanosheets that have unique metal ratios. The increase of the sensor material's electrochemical activity is mainly due to the Ni and Co synergistic interaction. In addition, changing the metal ratio may improve electro-catalytic activity. The most effective electrochemical performance for glucose sensing is found in Co/Ni-MOF nanosheets with a 2:1 Co-Ni ratio. The MOF nanosheet-based sensor material has a high affinity for glucose due to the stronger bonding interaction between the metal sites and the O atom in the analyte. The electrochemical oxidation of glucose is also enhanced by the synergistic effect at low applied voltage. The high surface area of the ultrathin structure allows analytes to make direct contact with the electrode surface, which is why all of the produced metal-organic framework nanosheets exhibited a low charge transfer resistance (>50Ω). The developed sensor functions effectively in actual sample analysis with 90.1% accuracy and has a wide linear range (0.1 M-1.4 mM), low detection limit (0.047 M) and very high sensitivity (2086.7 A mM^{-1} cm^{2}) (Varsha and Nageswaran 2020).

Table: 3 Review of the literature on electrochemical sensors made of two-dimensional MOF nanosheets.

Analyze	Material	LOD	LDR	References
miR3123	BPNSs/TH/Cu-MOF	0.3 pM	2 pM^{-2} μM	(Sun, Jin et al. 2020)
H_2O_2	AgNPs/Cu-TCPP	1.2 μM	3.7 μM-5.8 mM	(Ma, Bai et al. 2019)
Dopamine	PXa/Au/Cu-TCPP	1.0 μM	5–125 μM	(Qiu, Yang et al. 2019)
H_2O_2	Cu-TCPP/MWCNT	0.70 μM	0.001–8.159 mM	(Wang, Huang et al. 2019)
Mucin 1	521-MOF	0.12 pg ml^{-1}	0.001–0.5 ng ml^{-1}	(Wang, Huang et al. 2019)
Glucose	Ni-BDC 6.68	6.68 μM	0.01–0.8 mM	(He, Duan et al. 2017)
Hydrazine hydrate	Ni-MOF 0.5–96	0.23 μM	8000 μM	(He, Duan et al. 2017)
Glucose	Co-MOF	0.25 μM	0.5–8065.5 μM	(Li, Shao et al. 2019)
H_2O_2	AuCu/PPy/Cu-TCPP	6.67 nM	7.10μM–24.10 mM	(Zhang, Li et al. 2020)

H_2O_2	Ni-MOF/Hemin	0.2 μM	1 μM–0.4 mM	(Shu, Chen et al. 2019)
Glucose	Ni-MOF/NF	85 nM	0.04–2 mM	(Lu and Wu 2018, Ravipati, Durai et al. 2023)

Black phosphorous nanosheets (BPNSs), thionine (TH), graphitic carbon nitride (g-C_3N_4), nickel foam (NF), polypyrrole (PPy), poly(xanthurenic acid (PXa), tetrakis(4-carboxyphenyl)porphyrin (TCPP) and 521-MO are the abbreviations for these materials (Varsha and Nageswaran 2020).

3.2 Environmental Surveillance

Rapid industrialization and urbanization have a negative impact on the environment's ecology. The best way to identify dangerous substances is by creating effective electrochemical sensors, especially for the heavy metal ion detection in water and toxic fumes at low concentrations. Using MOF-based composites as fine sensing materials allows for the electrochemistry conversion of hazardous compounds found in the air and water. However, the size, shape and connectivity of the organic binders used to construct MOF have a significant impact on the formation of inorganic clusters. Therefore, it is essential to increase the variety and characteristics of MOF in order to employ them in environmental monitoring (Aslam, Ismail et al. 2014).

To detect glyphosate, work is being done on a multilayered porous Cu-benzene-1,3,5-tricarboxylic acid MOF. Because of the strong attraction between the chelate groups on the glyphosate and the Cu^{2+}, the synthetic material's reaction current was noticeably increased. Another example is the development of an electrochemical adapter sensor for Pb^{2+} detection employing MoS_2/rGO and AuPd@Fe-MOFs (gold-palladium modified iron-metal-organic frameworks) enhanced with gold. Improved detection performance is a result of the catalytic chain and base complementary combination. It's interesting that the desymmetrization technique produces the organic ligand that resembles a hinge. Due to molecular level modifications in MOF materials, the coexistence of acidic and alkaline places is a possibility. This functionally structured synthetic mesoporous composite aids in the transition to cascade catalytic processes by creating high activity of a two stage effective catalytic reaction in series (Feng, Wang et al. 2019).

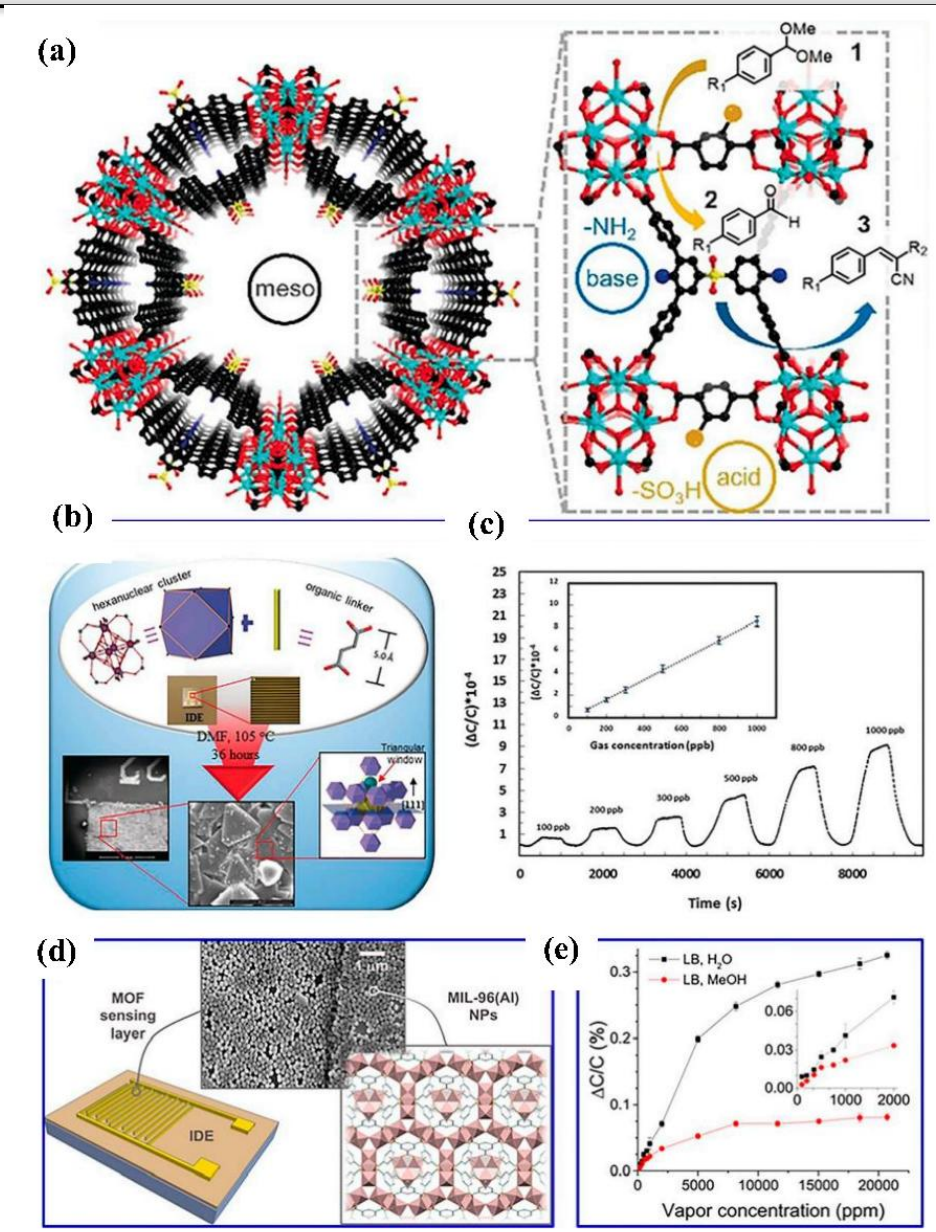

Figure: 7. (a) Using a bifunctional mesoporous catalyst, benzaldehyde dimethylacetal and malononitrile were combined in one pot. (Feng et al., 2019). (b) The fumarate-based fcu-MOF's prepared technique is shown schematically. (c) H_2S may be detected at values between 1 and 100 ppm (Yassine et al., 2016). (d) A diagram of the IDEs structure that depicts the MOF LB film's SEM characterization is employed (e) An illustration of the IDEs structure that shows how the MOF LB film is characterized by SEM (Andrés, Vijjapu et al. 2020)

As electrically transduced gas sensors, MOF based composites with outstanding gas adsorption/separation capabilities can be used. By using MOFs, interdigitated electrode chip-based capacitive sensors detection performance may be improved. For example, an in situ growing approach is used to create an interdigitated electrode using a fumarate based fcu-MOF thin film (Figure 7b). This recently constructed sensor (Figure 7c) has a low detection limit of around 5 ppb for H_2S and a high

detection sensitivity down to 100 ppb. MIL-96(Al) MOF thin films are also applied on interdigitated electrode chips using the Langmuir-Blodgett technique (Figure 7d) (Andrés, Vijjapu et al. 2020). These films may be improved to have greater selectivity and faster response/recovery for water as well as for detection of methanol, toluene, chloroform and other chemicals (Figure 7e) (Yao, Li et al. 2021).

3.3. Understanding the workings of antimicrobial MOFs

Even if a variety of antibacterial MOF compounds have been generated by various chemical procedures and synthetic reaction conditions, understanding the antibacterial processes of MOFs will surely make it simpler to discover antibacterial medications that perform better (Li, Liu et al. 2018). It is yet unclear, nonetheless, how MOFs most likely work against bacteria. One notion is based on the well-studied mechanism of action of metal oxide nanoparticles against bacteria. Bacterial cells cell walls and membranes may be harmed by the introduction of metal nanoparticles (NPs) (Slavin, Asnis et al. 2017). Reactive oxygen species (ROS), which are produced by the oxidative stress caused by the NPs are necessary for the damage-induced death of the bacterial cells (Figure 8). It is thought that MOF-anchored NPs work similarly against bacteria (Wyszogrodzka, Marszałek et al. 2016). In fact, recent studies have linked antibacterial action to the controlled release of metal ions via MOF disintegration. Furthermore, it has been shown that the controlled release of linkers produces the highly active organic ligands in MOFs, coordinating with the release of metal ions to enhance antibacterial activity (Lu, Ye et al. 2014). For instance, MOFs wide surface area and variety of porosities make them perfect for producing NPs with precise sizes, which is difficult to do with traditional metal NP synthesis techniques. MOFs structural stability and metal ion concentration both affect how effective they may be as antibiotics. Because of this, we focus on recent advancements in MOF-anchored nanoparticles and MOF-derived nanomaterials in this section for practical antibacterial applications. The many MOF-based compounds for bactericidal applications are investigated and their putative mechanisms of action are scrutinized in a number of significant studies (Table 4)

3.4. Antibacterial applications of MOFs

Biomedical research has recently put a lot of work into developing materials that can protect against bacterial infection in order to reduce difficulties encountered while medical care. To offer porous MOFs antibacterial qualities, researchers added antibacterial substances to their pores. In ideal pH circumstances and irradiation with UV radiation, rifampicin and 2-nitrobenzaldehyde (o-NBA), a pH jump reagent was effectively used to treat wound infections and cure in vivo and in vitro bacterial infections by inserting it into the pores of ZIF-8 (RFP&oNBA@ZIF-8). Noteworthy is the fact that, in optimal conditions, the RFP&o-NBA@ZIF-8 (rifampicin-o-nitrobenzoic acid-zeolitic imidazolate framework-8) material demonstrated strong antibacterial activity against gram-positive (methicillin-resistant Staphylococcus aureus, MRSA) as well as gram-negative (ampicillin-resistant Escherichia coli, E. (Song, Wu et al. 2018).

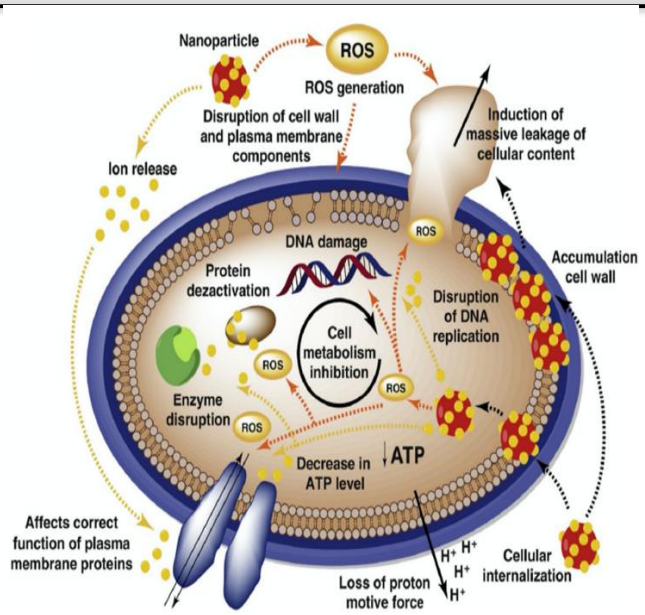

Figure: 8. Antimicrobial properties of metal-containing nanostructured systems (Wyszogrodzka, Marszałek et al. 2016).

Table 4: Various MOF-based compounds have bactericidal properties.

Metal-organic framework compound	Bactericidal action	Bacterial activity inhibitors	kind of microbe	References
[AgL]nnH_2O, L = 4-cyanobenzoate *	Oral bacteria: MIC = 21.17 lg/mL for all MOFs	Ag^+ ions	Oral bacteria	(Cao, Wu et al. 2020)
CP/CNF/ZIF-67	E. Coli: MIC = 10 lg/mL	Co^{2+} ions	E. Coli	(Qian, Lei et al. 2018)
Ag@CD-MOF	S. aureus: MIC = 64 lg/mL, MBC = 512 lg/mL	Ag NPs	E. Coli and S. aureus	(Shakya, He et al. 2019)
RFP&o-NBA@ZIF-8	E. Coli: MIC = 0–80 lg/mL	Zn^{2+} ions and RFP = rifampicin	E. Coli	(Song, Wu et al. 2018, Zhang, Zhang et al. 2024)
Ag@CD-MOF	E. Coli: MIC = 16 lg/mL, MBC** = 32 lg/mL	Ag NPs	E. Coli and S. aureus	(Shakya, He et al. 2019)
Cu3(NH2BTC)2-cotton	_	Cu^{2+} ions	E. coli	(Rubin, Neufeld et al. 2018)
RFP&o-NBA@ZIF-8	MRSA: MIC = 65–131 lg/mL	Zn^{2+} ions and RFP = rifampicin	MRSA	(Qian, Lei et al. 2018, Song, Wu et al. 2018)
Ag@Zn-BIF	E. Coli and S. aureus: MIC = 30–50 lg/mL	Ag NPs	E. Coli and S. aureus	(Qi, Ye et al. 2020)
HKUST-1/CS	_	Cu^{2+} ions	E. Coli and S. aureus	(Ren, Yang et al. 2019)
Cu10MOF	E. Coli and S. aureus:	Cu^{2+} ions	E. Coli and S.	(Han, Han et al.

	MIC = 500 ppm		aureus	2020)
MOF-5 and ZIF-8	Oral bacteria: MIC = 21.17 lg/mL for all MOFs	Zn^{2+} ions	Oral bacteria*	(Cao, Wu et al. 2020)

According to antibacterial activity investigations, the growth rate of E. coli was lowered by illumination for 120 minutes at a lowest the inhibiting mass of 10 mg mL^{-1}, whereas the MRSA MIC varied from 65 to 131mg mL^{-1}. According to in vivo experiments, the MOF material demonstrated exceptional antibacterial activity against bacterial infections at a pH of 8.5 when exposed to UV light (365 nm) (Figure 8). Because this MOF produces a local pH change and degrades into Zn^{2+} ions when exposed to UV light, it is essential for the regulated release of RFP. By combining MOFs with antibacterial substances, MOFs with wound-healing properties and antibacterial activity were produced. For instance, under controlled circumstances, MOF that break down to create Zn^{2+} ions when exposed to UV radiation may release RFP (Ryu, Jee et al. 2021).

3.5. Metal Ions Removal

The prevalence of heavy metal pollution, which makes water purification processes very challenging, is another issue with water treatment that has drawn a lot of attention. Increased toxicity and heavy metal ion bioaccumulation pose a major risk to the environment and general public's health. Because organic pollutants in industrial effluents often interact with heavy metals, their removal may be challenging. It has recently come to light that MOFs and their composites have the potential to remove heavy metals such as Pb(II), Cd(II), Cu(II), Ni(II) and others with effectiveness (Kumar, Singh et al. 2021). Although MOFs and their composites are beneficial for heavy metal removal, there is relatively little research on the effectiveness of MOF based photocatalytic membranes for this purpose. Adsorption plays a major role in the removal of heavy metals from MOF based photocatalytic membranes (Xu, An et al. 2021). The transformation of high valence heavy metal ions, such as As, Cr and U, into low-valence ions by photocatalytic reduction is advantageous for further processing. The resultant low valence heavy metal ions often precipitate as metal hydroxide, which aids in the deposition and immobilization of metal ions. The membranes containing UiO-66-NH_2(Zr/Hf) shown remarkable efficiency in reducing Cr(VI) under both simulated and actual UV exposure (Song, Jiang et al. 2019).

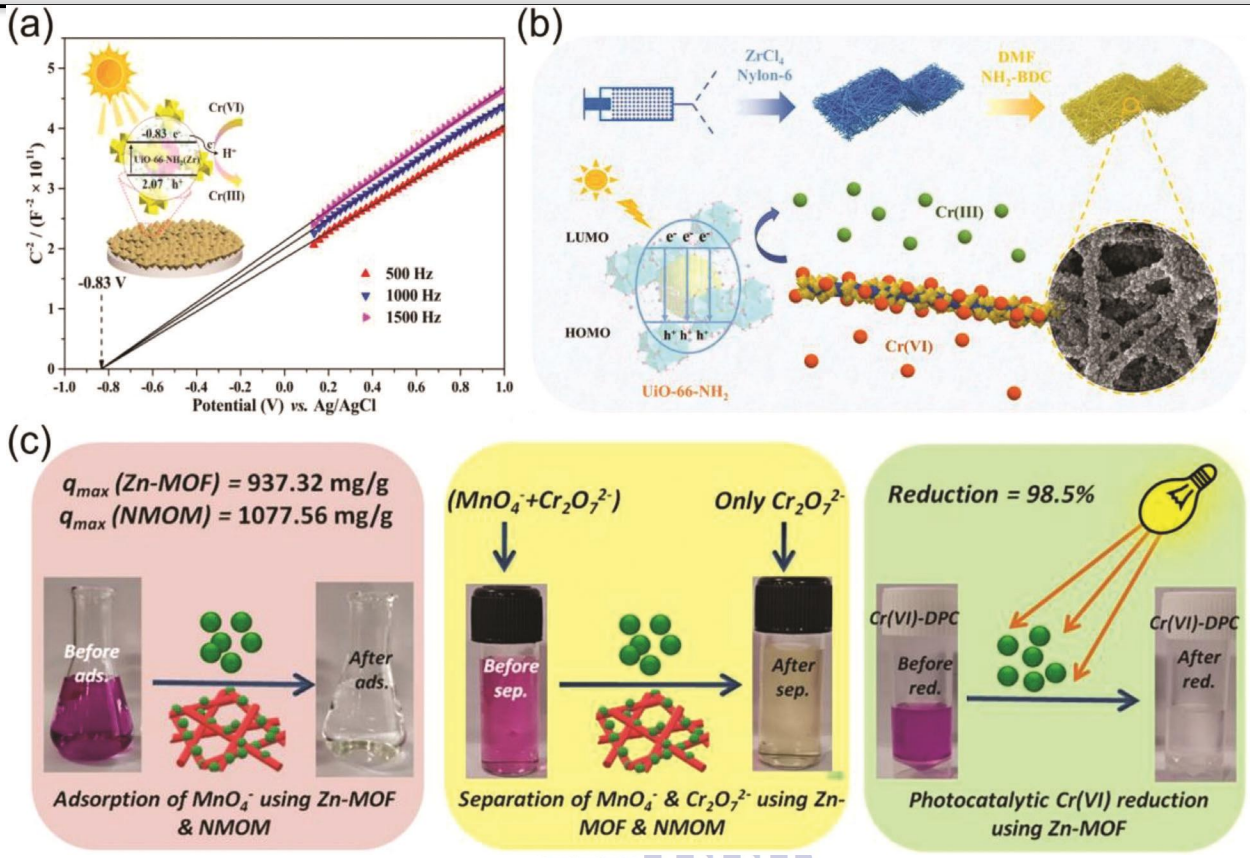

Figure: 9. a) The mechanism of the UiO-66-NH_2(Zr) membrane for photocatalytic reduction of Cr(VI) and the Mott-Schottky plot of UiO-66-NH_2(Zr) (Du, Yi et al. 2019). b) Diagrammatic representation of nylon-6@UiO-66-NH_2 fiber membrane adsorption photocatalysis reduction towards Cr(VI) (Zhang, Cao et al. 2022). c) An example of how to remediate pollutants based on oxo-anion utilizing Zn-MOF and NMOM (Kaur, Chandel et al. 2022).

The subsequent membranes had flat-band potentials of -0.83 and -0.92V, respectively and are designated UiO-66-NH_2(Zr) and UiO-66-NH_2(Hf). These results were more negative than the Cr(VI)/Cr(III) +0.51V range that might be attainable. Therefore, photo-induced electron transport for Cr(VI) reduction to Cr(III) on the UiO-66-NH_2(Zr) membrane proved thermodynamically feasible (Figure 9a). Even after 20 cycles, the UiO-66-NH_2(Zr) membrane demonstrated exceptional water and chemical stability, with a reduction efficiency of more than 94% for Cr(VI). However, it did not seem that the common foreign ions present in surface water had any negative impacts on Cr(VI) reduction. Afterwards, the effects of starting solution pH and different water sources on the reduction of Cr(VI) were investigated using CF/MoS_2/NH_2-MIL-125(Ti) cloth. (Xiao, He et al. 2017). They saw a drop in the clearance rate from 100% to 50.3% when the pH of the solution increased from 2.1 to 8.2. The usual behavior of Cr(VI) in acidic and alkaline environments, respectively, may be used to explain the observed phenomenon as $Cr_2O_{72}^-$ and CrO_{42}^-, respectively. $Cr_2O_{72}^-$ has been shown to be more susceptible to reduction than CrO_{42}^-. Furthermore, at alkaline conditions, the catalyst surface tended to get coated with $Cr(OH)_3$, which decreased the amount of interaction between the catalyst's active site and Cr(VI). Consequently, there was a decline in the effectiveness of Cr(VI) reduction. Compared to tap and lake water, the removal rate of Cr(VI) employing the composite material was maximum when deionized water

was employed as the water source. The presence of organic compounds in lake water and inorganic ions in tap water might perhaps provide an explanation for this (Kaur, Garg et al. 2024).

A nylon-6@UiO66-NH_2 fibre membrane with selective adsorption capacity was created in a recent work to aid in the photocatalytic reduction of Cr(VI) (Figure 9b). The suggested photocatalytic membrane had remarkable adsorption capacity for Cr(VI) (202.79 mg g^{-1}) due to strong electrostatic and chelation interactions, which aided in the reduction of Cr(VI) to Cr(III) when exposed to light. Furthermore, it was discovered that the nylon-6@UiO-66NH_2 fibre membrane exhibited a photocatalytic capacity for Cr(VI) of about 27.1 mg g^{-1} of UiO-66-NH_2, almost twice that of the pure UiO-66-NH_2 powder (15.5 mg g^{-1}) (Ji, Wang et al. 2023). The MOF-based photocatalytic membrane may also have the ability to selectively adsorb other detrimental oxo-anions, such as MnO_4^-. A study on the purification of oxo-anions in aqueous solution utilizing Mercapto-decorated Zn-MOF modified membrane (NMOM) was carried out (Kaur, Chandel et al. 2022). The researchers found that the virgin Zn-MOF and NMOM could preferentially adsorb MnO_4^- in aqueous solution, making it easier to separate MnO_4^- from the mixture of MnO_4^- and $Cr_2O_{72}^-$. The adsorption capacities of virgin Zn-MOF and NMOM were 937.32 and 1077.56 mg g^{-1}, respectively. Both pure Zn-MOF and NMOM demonstrated significant adsorption capabilities, with values of 937.32 and 1077.56 mg g^{-1}, respectively. Notably, the Zn-MOF proved its potential as an effective catalyst, allowing the photocatalytic reduction of $Cr_2O_{72}^-$ to Cr(III) with an incredible 98.5% conversion rate (Figure 9c). These findings indicated that a potential use for MOF-based membranes is the elimination of heavy metal contaminants from water sources (Goudarzi, Khosroshahi et al.).

3.6. Light-emitting diodes (LEDs)

In LED applications, LMOFs remarkable photoluminescence behavior has been widely used. Indeed, multiple channels of energy or charge transfer resulting from MOF structure-property coupling can produce photoluminescence. In order to improve and tune the luminescence characteristics, Practical approaches such are combinations of metal ligands, the addition of multifunctional moieties to the MOF system and the immobilization of luminous guest molecules are highly stressed. Highlighted are the latest developments in lanthanide metal-organic frameworks (LMOFs) for use in light-emitting diode (LED) applications (Kaur, Sundriyal et al. 2019).

3.7. Organic Pollutant Degradation

The removal of organic pollutants from water may be a challenging task due to their diverse nature. Eliminating and successfully controlling organic contaminants is one of the main objectives of water treatment. Photocatalytic membranes provide for both photocatalytic degradation and excellent rejection of organic contaminants (Dhivya, Magadevan et al. 2019). The capacity of MOF-based photocatalysts to generate reactive oxygen species (ROS) like $^{\cdot}O_2^-$ and $^{\cdot}OH$ when exposed to visible light determines the degradation of organic contaminants (Cao, Zhang et al. 2021). The processes of morphological control, ligand functionalization, metal ion doping, MNP modification, hetero-structure formation and defect management may all be employed to increase MOF's photocatalytic capability by promoting the separation of photoinduced electrons and holes. We have already discussed the methods and outcomes of various alteration strategies. Zn-TCPP functionalized polyamide membrane laminates, for example, (Xu, Feng et al. 2021) visible light energy that is equivalent to or higher than the energy band gap between the two may drive Zn-TCPP electrons from the VB to the CB. The electrons may react with the surrounding O_2 and H_2O after they reach the CB, creating $^{\cdot}OH$ radicals.

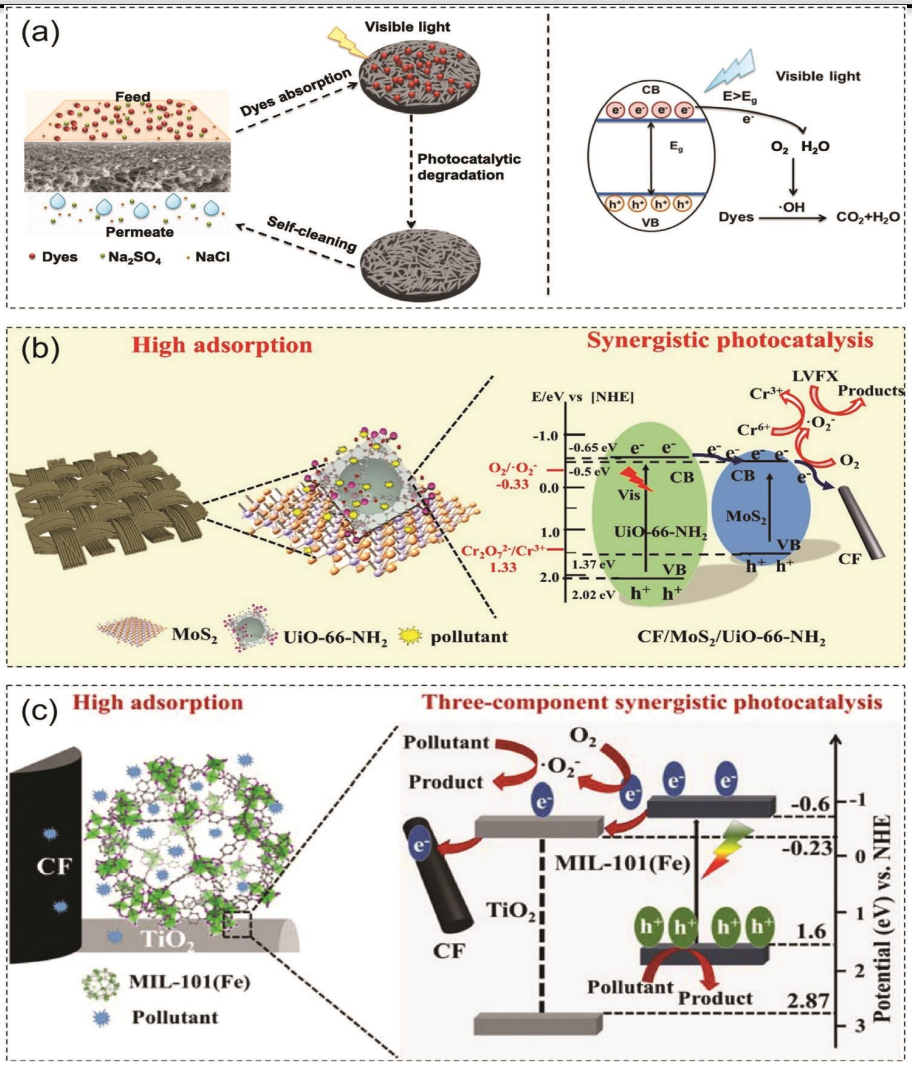

Figure: 10. a) Zn-TCPP laminates are filtered and then photodegraded to produce functionalized polyamide membranes. (Xu, Feng et al. 2021). b) The CFs/MoS_2/UiO-66-NH_2 fabric's adsorption and photocatalysis mechanism (Cao, Zhang et al. 2021). c) Diagrammatic illustration of the CFs/TiO_2/MIL-101(Fe) cloth photocatalytic mechanism and adsorption (Zhang, Xiong et al. 2021).

These radicals have the power to oxidize organic colors to tiny molecules like CO_2 and H_2O, which will eventually remove the associated dye pollutants that cause membrane fouling (Figure 10a). In addition, the substrate membrane is essential for getting rid of organic contaminants. First off, the capacity of the membrane to reject impurities is essential to guaranteeing the efficient elimination of organic contaminants. The two primary methods of separation that are well recognize are size sieving and electrostatic effects. Pollutants that are larger than the pores in the membrane and those that repel electrostatically to the membrane surface are more likely to be caught (Zhou, Feng et al. 2021). (Figure 10b) Second, by extending the duration of interaction between pollutants and photocatalysts on the membrane, the membrane rejection process promotes the complete destruction of the molecules of organic pollutants that are rejected. Additionally, a lot of loading sites and good chemical stability are often found in substrate membranes or modified substrate membranes, which efficiently fix MOF photocatalysts and provide MOF stability during the formation of free radicals, preventing the leaching

of hazardous metal ions (Sun, Zucker et al. 2018). Finally, materials for the membrane that have a hierarchical porous structure facilitate light refraction and reflection across the membrane, which enables interior MOF to take part in the photocatalytic process. As light is reflected back through the film's helical pores, the photocatalyst in the membrane absorbs additional light (Figure 10c) (Chen, Fei et al. 2024). Because of these advantages, MOF photocatalytic film outperforms MOF photocatalytic particles in terms of photocatalytic activity, stability and mobility, enabling useful sewage treatment applications (Shi, Huang et al. 2019, Chen, Fei et al. 2024).

3.8. 2D MOFs in Electrocatalysis

The surfaces of the materials play a crucial role in the electrocatalytic processes and greatly influence their outcome. The flexible surface and active areas for electrocatalysis of 2D MOF materials provide a chance to develop an effective electrode. The use of 2D MOFs in real-world scenarios is constrained by a number of issues, including as instability, limited conductivity and aggregation. Conversely, the many active sites, electrode adhesion ability and structural adaptability of many 2D MOF derivatives signify the unique benefits of electrocatalysis. As a result, the adjustable atomic surfaces, quick mass transport, plenty of active sites and enhanced charge transfer of ultrathin 2D MOF nanosheets and their derivatives make them very efficient catalysts. The development of 2D MOF electrocatalysts for HER, OER and other general water-splitting applications is reviewed in this paper (Khan, Nairan et al. 2023). Table 5 summarizes the electrochemical performance of materials made from 2D MOFs as reported in recent studies.

Table 5. Tafel slopes and summarised overpotentials of 2D MOF electrocatalysts that have been published in the literature (η: overpotential at 10 mA cm^2, CC: carbon cloth, RDE: rotating disc electrode, GCE: glassy carbon electrode, SSE: self-supported electrode)

Catalyst Name	Electrolyte	Substrate	η [mV]	Tafel slope [mV dec^{-1}]	References
HER electrocatalysts					
Ni MOF derived N-HCGHF	1.0 M KOH	GCE	95	57	(Yan, Xu et al. 2020)
Ni MOF/Pt	0.5 M H_2SO_4	GCE	43	30	(Rui, Zhao et al. 2019)
Pt NC/Ni MOF	1.0 M KOH	GCE	25	42.1	(Zhu, Qiao et al. 2020)
Co MOF/H_2	1.0 M KOH	NF	30	88	(Xia, Liu et al. 2020)
ZIF derived Co-NC@10rGO	1.0 M KOH	NF	220	128	(Arunkumar, Gayathri et al. 2024)
3ZIF-67 derived Pt/RGO	1.0 M KOH	RDE	37.2	33.1	(Wu, Zhang et al. 2020)
3ZIF-67 derived Pt/RGO	1.0 M KOH	RDE	37.2	33.1	(Wu, Zhang et al. 2020)
$Ni_3(Ni_3$·HAHATN$)_2$	0.1 M KOH	RDE	115	45.6	(Huang, Zhao et al. 2020)

OER electrocatalysts					
Te, Cl-NiFe/NF	1.0 M KOH	SSE	224 [30 mA cm^2]	37.6	(Park, Kwon et al. 2022)
$Co_3(HITP)_2$	1.0 M KOH	CC	254	86.5	(Xing, Wang et al. 2020)

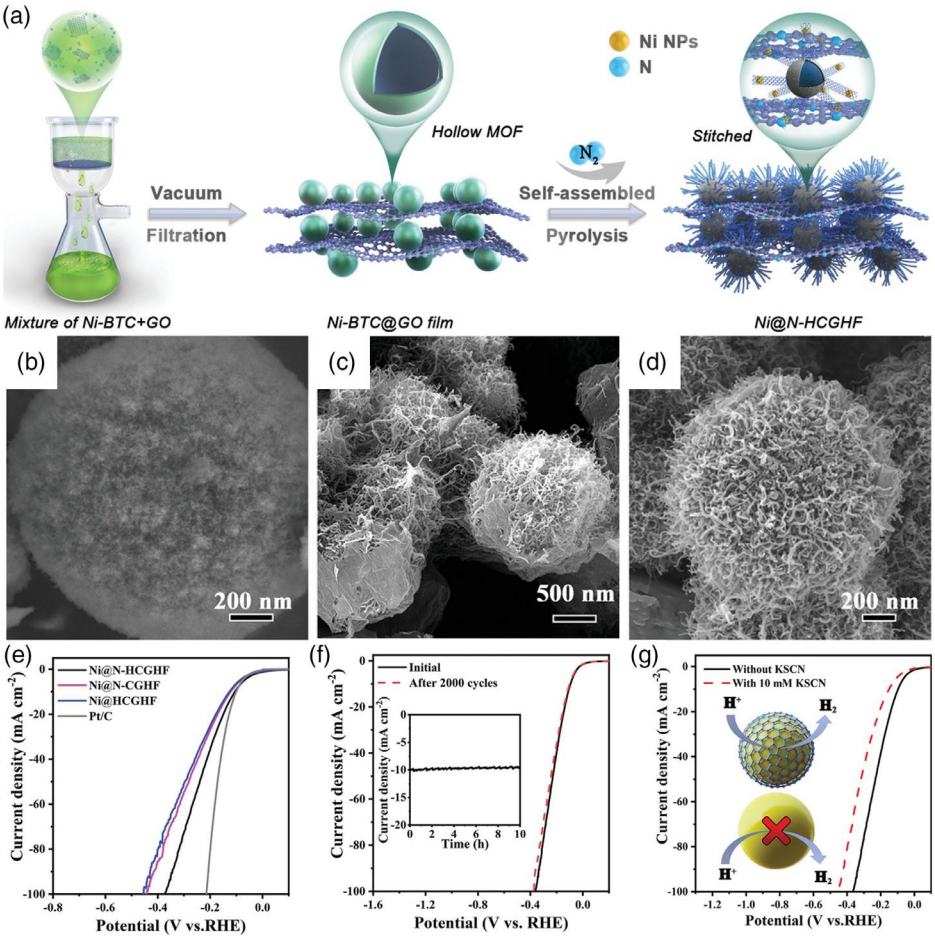

Figure 11. a) Diagram of N-doped graphene oxide heterostructure film (HNCGHF)/hollow carbon nanotubes (CNT) Ni-MOF (Ni@N-HCGHF). b) Hollow Ni-BTC spheres: their morphology. c) Perspective of Ni@N-HCGHF in cross-section. d) hollow structure of N-doped CNTs on MOF. e) Linear sweep voltammetry (LSV) plots for hydrogen evolution reaction (HER). f) Ni@N-HCGHF LSV plots both before and after cyclic voltammetry (CV) cycles. g) Ni@N-HCGHF LSV maps both before and after KSCN immersion (Yan, Xu et al. 2020)

The HER (Hydrogen Evolution event), a critical event that has drawn a lot of attention, produces enormous volumes of very pure hydrogen. Electrochemical techniques, which are considered to be the most interesting way to make hydrogen, are currently the most feasible and effective approach to split water into hydrogen and oxygen. The electrocatalytic performance in HER is correlated with the catalyst on the electrode. Thus, in order to speed the reaction kinetics and enable effective HER, the

electrocatalysts must be advanced. These days 2D MOFs have attracted a lot of attention from HER electrocatalysts because of their small thickness and wide surface area for many active sites to boost electrocatalysis effectiveness. The schematic depiction of the Ni@N-HCGHF is shown in Figure 11a, which shows the large-scale manufacturing of the graphene oxide (GO)/N-doped hollow carbon nanotubes (CNTs) heterostructure film Ni-MOF. Initially, the MOF was fabricated from Ni-BTC hollow spheres by means of a conventional solvothermal technique. Trimesic acid (H_3BTC), nickel nitrate ($Ni(NO_3)_2 \cdot 6H_2O$) and PVP were usually combined in a solution and subjected to a hydrothermal procedure in an autoclave lined with Teflon for six hours at 150 °C. The form of hollow Ni-BTC spheres is shown in Figure 11b. The filtering process helped to create a continuous film after the Ni-BTC and GO solution had been vigorously stirred and sonicated. As Figure 11c shows, dicyandiamide was used in conjunction with thermal treatment of the resulting film to synthesize Ni@N-HCGHF. N-doped CNTs were sewed together with reduced GO nanosheets (N-CNT@rGO) to form a porous 3D carbon matrix network. The N-CNT hollow structure formed from MOF, as shown in Figure 11d, provided a wide surface area to generate several active sites for catalysis. The conventional three electrode setup was used to conduct the electrochemical catalytic property analysis in 1M potassium hydroxide (KOH). The catalyst's distinct structure and predicted composition served as the driving forces for this experiment. The linear sweep voltammetry (LSV) curves in Figure 11e showed a modest over potential of 95 mV at 10 mA cm^{-2}. The analysis of a minor instability of the electrocatalyst (Ni@N-HCGHF) during 2000 cycles of cyclic voltammetry is shown in Figure 13f. Metal active site poisoners called thiocyanate ions were dissolved in 1M KOH to ascertain the materials outperform activity. It was discovered that the electrocatalyst's performance remained higher than that of the majority of non-nobel-metal catalysts, demonstrating the catalyst's exceptional catalytic activity (Yan, Xu et al. 2020).

Summary

Among the present difficulties that 2D MOFs face are the following:

1) Even while 2D MOF-related materials have higher surface areas and surface active sites than 3D MOF materials, their weak structure and low stability prevent them from being used in practical applications.
2) Conductivity may still be greatly improved in 2D MOFs, which are often semiconductors or insulators.
3) It is still necessary to think of more appropriate methods for the controllable synthesis of monolayer, high-quality MOFs. Target MOF design is made more challenging by the uncertainty of conformational interactions and the necessity to further investigate the chemical reaction processes of MOF-related materials.

The following are some practical suggestions for creating synthetic target 2D MOFs:

One should concentrate on controlling the kinetic and thermodynamic factors throughout the crystallization process in order to properly regulate the size and form of the MOF nanostructures. For example, if the reaction rate is changed too rapidly, many molecules will group together and be unable to create a two-dimensional structure. Moreover, a high temperature will destroy the porosity, while a low temperature would increase the material's thickness. The most researched approach at the moment, which provides new ideas for creating and manufacturing innovative materials, is simulating machine learning algorithms to predict important variables including the electrical characteristics, pore structure and 2D MOF crystal form.

Redox-inert organic ligands, which are the primary sources of electrical conductivity loss, bind metal ions together. In order to create covalent bonds, metal ions and organic ligands with loosely bound electrons were used in two ways: first, to overlap the proper high-energy and spatial orbitals and second, to facilitate charge transfer. Because MOFs are porous, redox-active guest molecules may be inserted as

charge carriers or, via guest-frame interactions, employed as charge dopants. New ideas for this path are offered by current research on bimetallic MOFs, which introduces two distinct metal ions into the framework to produce additional metal-metal connections with high conductivity. Certain bimetallic organic frameworks exhibit charge transfer or electron sharing between the two metal ions, creating more conductive channels and enhancing the material's conductivity. Despite the aforementioned difficulties, 2D MOF-based materials have appealing qualities. As research and development continue, more internal guidelines will become clear, novel approaches to the synthesis of particular MOF will be used, and certain issues may be effectively resolved. It is anticipated that 2D MOF based materials have a huge development potential. New insights into the thoughtful synthesis and design of 2D MOFs are provided by this review.

This study outlines current advancements in the production of 2D layered MOF nanosheets and their uses in electrochemical sensing and electrocatalysis. A brief introduction to the various top-down and bottom-up synthetic methodologies for 2D MOF preparation has been provided. Sonication is one of the most used top-down techniques for exfoliating 3D bulk MOF. The top-down technique has a number of benefits, but its practical applicability is limited by its poor yield and the instability of exfoliated sheets. Combining the two techniques and using solvents with a surface energy comparable to that of MOF can increase yield and stop layers from restacking, respectively. Bottom-up synthesis, as opposed to top-down synthesis, involves directly synthesizing MOF from its precursors. This allows for the controlled development of MOF by the adjustment of precursor composition and synthetic circumstances. Nonetheless, it is important to develop further simple synthetic techniques for high-quality 2D MOF. Nearly every 2D MOF nanosheet material created to date for electrochemical sensing applications is summed up in this overview. We are still in the early stages of using 2D MOF as electrode material for sensing. For MOF-based sensors to be successfully fabricated, a number of issues must be resolved. Even with the development of several techniques for growing ultrathin 2D MOF nanosheets, there are still many unanswered questions about the large-scale, controlled synthesis of these materials with excellent quality, high yield, good stability, and high production rate. MOF's non-uniform shape presents uncertainties for catalytic performance and structural analysis. When 2D MOFs or MOF-derived nanosheets are fully developed, they will have huge lateral diameters, regulated directional growth, and uniform morphologies for catalytic applications. Long-term stability and an exceptionally low overpotential are necessary for effective electrocatalysts in order to be used in devices and energy storage applications. We anticipate that scientists working in the fields of 2D MOF and energy and conversion devices will find great value in this mini-review.

References

1. Abhervé A, Mroweh N, Cauchy T, Pop F, Cui H, Kato R, Vanthuyne N, Alemany P, Canadell E, Avarvari NJJMC C. Conducting chiral nickel (ii) bis (dithiolene) complexes: structural and electron transport modulation with the charge and the number of stereogenic centres. 2021;9(12):4119-4140.
2. Ahsan MA, He T, Eid K, Abdullah AM, Sanad MF, Aldalbahi A, Alvarado-Tenorio B, Du A, Puente Santiago AR, Noveron JCAA M. Controlling the interfacial charge polarization of MOF-derived 0D–2D vdW architectures as a unique strategy for bifunctional oxygen electrocatalysis. 2022;14(3):3919-3929.
3. Amo-Ochoa P, Welte L, González-Prieto R, Miguel PJS, Gómez-García CJ, Mateo-Martí E, Delgado S, Gómez-Herrero J, Zamora FJC C. Single layers of a multifunctional laminar Cu (I, II) coordination polymer. 2010;46(19):3262-3264.
4. Andrés MA, Vijjapu MT, Surya SG, Shekhah O, Salama KN, Serre C, Eddaoudi M, Roubeau O, Gascón IJAAM interfaces. Methanol and humidity capacitive sensors based on thin films of MOF nanoparticles. 2020;12(3):4155-4162.
5. Araki T, Kondo A, Maeda KJC C. The first lanthanide organophosphonate nanosheet by exfoliation of layered compounds. 2013;49(6):552-554.
6. Arunkumar P, Gayathri S, Rajasekar A, Kumar SS, Kamaraj SK, Han JHJ oCS I. Lewis acidic Fe3+-driven catalytic active Ni3+ formation in Fe-free metal–organic framework for enhanced electrochemical glucose sensing. 2024; 656:424-439.
7. Ashworth DJ, Foster JAJJMC A. Metal–organic framework nanosheets (MONs): a new dimension in materials chemistry. 2018;6(34):16292-16307.
8. Aslam M, Ismail IM, Almeelbi T, Salah N, Chandrasekaran S, Hameed AJC. Enhanced photocatalytic activity of V2O5–ZnO composites for the mineralization of nitrophenols. 2014; 117:115-123.
9. Aykanat A, Meng Z, Stolz RM, Morrell CT, Mirica KAJA CIE. Bimetallic Two-Dimensional Metal–Organic Frameworks for the Chemiresistive Detection of Carbon Monoxide. 2022;61(6): e202113665.
10. Bauer T, Zheng Z, Renn A, Enning R, Stemmer A, Sakamoto J, Schlüter A DJACIE. Synthesis of free-standing, monolayered organometallic sheets at the air/water interface. 2011;50(34):7879-7884.
11. Cao F, Zhao M, Yu Y, Chen B, Huang Y, Yang J, Cao X, Lu Q, Zhang X, Zhang ZJACS. Synthesis of two-dimensional CoS1.097/nitrogen-doped carbon nanocomposites using metal–organic framework nanosheets as precursors for supercapacitor application. 2016;138(22):6924-6927.
12. Cao P, Wu X, Zhang W, Zhao L, Sun W, Tang ZJIC R. Killing oral bacteria using metal–organic frameworks. 2020;59(4):1559-1567.
13. Cao W, Zhang Y, Shi Z, Liu T, Song X, Zhang L, Wong PK, Chen ZJCE J. Boosting the adsorption and photocatalytic activity of carbon fiber/MoS2-based weavable photocatalyst by decorating UiO-66-NH2 nanoparticles. 2021; 417:128112.

14. Cardoso SPP. Synthesis and Characterization of Small Pore Membranes and Their Application to the Separation of Hydrogen Containing Mixtures. Universidade de Aveiro (Portugal); 2019.
15. Chai L, Pan J, Hu Y, Qian J, Hong MJS. Rational Design and Growth of MOF-on-MOF Heterostructures. 2021;17(36):2100607.
16. Chang C, Chen W, Chen Y, Chen Y, Chen Y, Ding F, Fan C, Fan HJ, Fan Z, Gong CJAPCS. Recent progress on two-dimensional materials. 2021;37(12):2108017.
17. Chen C, Fei L, Wang B, Xu J, Li B, Shen L, Lin HJS. MOF-Based Photocatalytic Membrane for Water Purification: A Review. 2024;20(1):2305066.
18. Chen I-F, Lu C-F, Su W-FJL. Highly conductive 2D metal–organic framework thin film fabricated by liquid–liquid interfacial reaction using one-pot-synthesized benzenehexathiol. 2018;34(51):15754-15762.
19. Chen S, Dai J, Zeng XCJPCC P. Metal–organic Kagome lattices M3 (2,3,6,7,10,11-hexaiminotriphenylene)2 (M= Ni and Cu): from semiconducting to metallic by metal substitution. 2015;17(8):5954-5958.
20. Cheng J, Yang X, Yang X, Xia R, Xu Y, Sun W, Zhou JJFPT. Hierarchical Ni3S2@2D Co MOF nanosheets as efficient hetero-electrocatalyst for hydrogen evolution reaction in alkaline solution. 2022; 229:107174.
21. Chhowalla M, Shin HS, Eda G, Li L-J, Loh KP, Zhang HJN. The chemistry of two-dimensional layered transition metal dichalcogenide nanosheets. 2013;499(7457):419-425.
22. Choi H, Ko K-C, Park S, Lee JYJC. Rational design of porous conjugated polymers and metal–organic frameworks for photocatalytic water splitting under visible light. 2016;18(7):791-824.
23. Choi H, Ko K-C, Park S, Lee JYJC. Rational design of porous conjugated polymers and metal–organic frameworks for photocatalytic water splitting under visible light. 2016;18(7):791-824.
24. Choi J, Lee J, You J, Kim J, Nam DH, Kim S, Yoo DK, Kim J, Lee JS, Kim SKJCE J. Highly selective gas sensor using a metal–organic framework with mesoporous channel. 2020; 398:125597.
25. Choi S, Ko NR, Lee H, Kim H, Oh MJA. Synthetic Conditions Control Morphologies of Iron Phosphonates: From Hollow Microspheres Composed of Nanoplates to Unusual Interpenetrated Frameworks. 2015;127(40):13584-13590.
26. Choudhury A, Nandi A, Chowdhury H, Saha SJC. Electrochemical performance of reduced graphene oxide-MnO2 nanocomposites for supercapacitor application. 2014; 116:364-370.
27. Chui SS-Y, Lo SM-F, Charmant JP, Orpen AG, Williams IDJ S. A chemically functionalizable nanoporous material [Cu3(TMA)2(H2O)3] n. 1999;283(5405):1148-1150.
28. Clough AJ, Yoo J, Mecklenburg MH, Marinescu SCJC. Two-dimensional metal–organic surfaces for efficient hydrogen evolution from water. 2015;137(1):118-121.
29. Cohen SMJCR. The postsynthetic renaissance in porous solids. 2012;112(2):970-1000.
30. Colon YJ, Snurr RQJC. High-throughput computational screening of metal–organic frameworks. 2014;114(12):12496-12535.
31. Cui X, Xu H, Li H, Li D, Gao L, Li H, Li H, Gao L, Li D, Xu HJN. Metal–organic framework nanocrystals for energy storage and conversion. 2016;1(6):16024.
32. Cui Y, Yue Y, Qian G, Chen BCC. Luminescent functional metal–organic frameworks. 2012;112(2):1126-1162.
33. Culp JT, Smith MR, Goodman A, Frenkel AI, Pellegrini KL, Fodor J, McDonnell S, Hill CL, Peterson GW, DeCoste JBJAEM. Postsynthetic modification of a metal–organic framework to introduce active surface sites for gas adsorption. 2013;3(2):349-356.

34. Dai J, Zeng X CJJotACS. Titanium tris (dithiolene) monolayers: Two-dimensional Dirac materials with high Fermi velocities. 2014;136(16):5595-5598.
35. D'Alessandro DMJCR. Exploiting redox activity in metal–organic frameworks: concepts, trends and perspectives. 2016;116(2):598-664.
36. Dincă M, Long JRJACIE. Hydrogen storage in microporous metal–organic frameworks with exposed metal sites. 2008;47(36):6766-6779.
37. Dong R, Han P, Arora H, Ballabio M, Karakus M, Zhang Z, Shekhar C, Adler P, Petkov P, Erbe AJNC. High-mobility band-like charge transport in a semiconducting two-dimensional metal–organic framework. 2018;9(1):1-9.
38. Dong R, Pfeffermann M, Strunk T, Liu F, Fritzsche M, Koitz R, Serafin M, Mena-Osteritz E, Doltsinis NL, Feng XJN. Large-area, free-standing, two-dimensional supramolecular polymer single-layer sheets for highly efficient electrocatalytic hydrogen evolution. 2013;4(4):296-302.
39. Dou J-H, Arguilla MQ, Luo Y, Li J, Zhang W, Sun L, Mancuso JL, Yang L, Chen T, Parent LRJN. Atomically precise single-crystal structures of electrically conducting 2D metal–organic frameworks. 2017;6(11):978-985.
40. Dou J-H, Sun L, Ge Y, Li J, Kamp M, Huang X, Chen L, Shang M, Dong R, Mandrus DJJACS. Signature of metallic state in a semiconducting metal–organic framework: The case of Ni3(HITP)2. 2017;139(39):13608-13611.
41. Duan J, Chen S, Jaroniec M, Qiao SZZ. Porous C3N4 nanolayers@ N-graphene films as catalyst electrodes for highly efficient hydrogen evolution. 2015;5(6):4810-4817.
42. Dutta S, Kim J, Uchida T, Matsumura D, Ariga K, Yamauchi YJAM. 2D nanosheets with nanoporosity: flake-like MOF-derived nanostructures for hydrogen evolution electrocatalysis. 2019;31(51):1905048.
43. Dutta S, Sahoo R, Das N, Pradhan MJPt. Recent advances in the design of metal–organic frameworks for electrochemical hydrogen evolution reaction. 2021;12(3):629-646.
44. Dutta S, Sahoo R, Pradhan MJC. Recent Advances in Metal–Organic Framework (MOF) Derived Electrocatalysts for Oxygen Evolution Reaction (OER). 2022;10(3):719-735.
45. Dutta S, Sahoo R, Pradhan MJC. Recent advances in metal–organic framework (MOF) derived electrocatalysts for oxygen reduction reaction (ORR). 2022;10(6):1904-1925.
46. Eddaoudi M, Kim J, Rosi N, Vodak D, Wachter J, O'Keeffe M, Yaghi OMJS. Systematic design of pore size and functionality in isoreticular MOFs and their application in methane storage. 2002;295(5554):469-472.
47. Falcaro P, Ricco R, Yazdi A, Imaz I, Furukawa S, Maspoch D, Ameloot R, Evans JD, Doonan CJNM. Application of metal and metal oxide nanoparticles@ MOFs. 2016;15(9):671-687.
48. Fan Y, Zhang Y, Guo H, Jiang X, Yu C, Xu H, Li H, Li D, Zhang L, Gao LJN. Engineering of MOF-derived CoP@ C–C nanocomposites as efficient electrocatalysts for hydrogen evolution reaction. 2018;9(6):861-870.
49. Feng D, Gu Z-Y, Li J-R, Jiang H-L, Wei Z, Zhou H-CJACIE. Zirconium-metalloporphyrin PCN-222: mesoporous metal–organic frameworks with ultrahigh stability as biomimetic catalysts. 2012;51(42):10307-10310.
50. Feng D, Lei T, Lukatskaya MR, Park J, Huang Z, Lee M, Shaw L, Chen S, Yakovenko AA, Kulkarni AJNM. Robust and conductive two-dimensional metal–organic frameworks with exceptionally high volumetric and areal capacitance. 2018;17(12):1072-1077.

51. Feng D, Wang K, Wei Z, Chen Y-P, Simon CM, Arvapally RK, Martin RL, Bosch M, Sun C, Yuan DJNM. Kinetically tuned dimensional augmentation as a versatile synthetic route towards robust metal–organic frameworks. 2016;15(1):68-72.
52. Furukawa H, Cordova KE, O'Keeffe M, Yaghi OMJCR. The chemistry and applications of metal–organic frameworks. 2013;112(2):1126-1162.
53. Furukawa H, Ko N, Go YB, Aratani N, Choi SB, Choi E, Yazaydin AÖ, Snurr RQ, O'Keeffe M, Kim JJSCI. Ultrahigh porosity in metal–organic frameworks. 2010;329(5990):424-428.
54. Furukawa S, Reboul J, Diring S, Sumida K, Kitagawa SJCCR. Structuring of metal–organic frameworks at the mesoscopic/macroscopic scale. 2014;48(4):1700-1734.
55. Gangu KK, Maddila S, Mukkamala SB, Jonnalagadda SBJC. A review on contemporary metal–organic framework materials. 2016; 46:1-36.
56. Geng K, He T, Liu R, Dalapati GK, Tan KTT, Li Z, Tao S, Gong Y, Jiang Q, Jiang DCC. Covalent organic frameworks: design, synthesis, and functions. 2020;120(16):8814-8933.
57. Ghosh S, Ghosh A, Rajeswari R, Natarajan SJC. Metal–organic framework nanosheets: synthesis methods and applications. 2020; 74:1-30.
58. Ghosh SK, Bharadwaj PKJACIE. Metal–organic framework nanosheets (MONs): a new dimension in materials chemistry. 2015;54(2):646-651.
59. Gong W, Chen H, Jiang H, Wang X, Chen X, Guo J, He J, Yang X, Wang YJMC. Zr-MOF nanosheet membranes for highly efficient ion sieving and water desalination. 2019;27(6):1206-1213.
60. Gu Z-Y, Yan X-PJA CS. Metal–organic frameworks for advanced applications in gas storage, separation, and catalysis. 2012;134(24):10569-10583.
61. Guo X, Zhu Y, Wang S, Chen Y, Li H, Shi Z, Xu Q, Zhang HJAM. Zr-based metal–organic framework hollow nanostructures as efficient photocatalysts for hydrogen production. 2018;30(20):1800004.
62. Guo Y, Zhao Y, Yu K, Zhou Y, Wu F, Yu GJAM. Engineering porous MOF-derived materials for advanced electrocatalysis. 2019;31(32):1901997.
63. Guo Z, Zhang H, Yu Z, Li J, Yang J, Wang J, Wang Y, Xu Q, Sun J, Zhao YJMC. Ultrathin 2D metal–organic framework nanosheets with high conductivity and electrocatalytic activity for the oxygen evolution reaction. 2019;27(14):2705-2711.
64. Han X, Huang J, Yuan D, Drake H, Jiang H-L, Wang C, Zhou H-CJACS. Chiral porous metal–organic frameworks with high stability for enantioselective separation and catalysis. 2019;141(19):7806-7815.
65. Han X, Ling X, Wang Y, Ma D, Li D, Liu Q, Chen H, Huang H, Zhong C, Zhang XJAM. Atomically thin 2D metal–organic framework nanosheets with a large lateral size for efficient catalysis. 2019;31(6):1804019.
66. Han X, Yang S, Liu L, Dong S, Zhang F, Wang Y, Zhao H, Wang C, Sun L, Song YJMC. Ultrathin 2D nanosheets of metal–organic frameworks for advanced electrochemical energy storage devices. 2018;26(45):8704-8710.
67. Hao J-N, Yan BJC. A dual-emitting water-stable lanthanide–organic framework as a self-calibrating luminescent sensor for detecting antibiotics. 2016;22(37):16275-16281.
68. He H, Sun F, Borjigin T, Zhu GJMC. Multifunctional lanthanide metal–organic frameworks: luminescent, magnetic, and catalytic properties. 2014;22(3):323-329.
69. He T, Ni B, Zhang H, Gong Y, Zhong Y, Wang X, Gu L, Hu J-S, Wan L-JJACS. MOF-derived Co–N–C electrocatalysts for high-performance oxygen reduction reaction. 2018;140(47):15493-15500.
70. He Y, Zhou W, Qian G, Chen BJMC. Metal–organic frameworks for luminescence thermometry. 2016;24(35):16723-16734.

71. Hu J, Chen Y, Wang J, Li C, Jiang H-LJACS. Porphyrinic MOFs as heterogeneous photocatalysts for CO2 reduction under visible light. 2015;137(47):15008-15015.
72. Hu J, Wang K, Li B, Zhang S, Gao H, Zhang S, Ma SJC. Recent advances in MOF-based photocatalysis for environmental applications. 2017;49(15):15255-15270.
73. Hu Z, Deibert BJ, Li JCMR. Luminescent metal–organic frameworks for chemical sensing and explosive detection. 2014;44(1):87-99.
74. Huang H, Li J, Wang K, Han T, Tong M, Li B, Zhou H-CJACS. An in situ self-assembly template strategy for the preparation of hierarchical-pore metal–organic frameworks. 2018;140(32):11519-11525.
75. Huang N, Wang P, Jiang DJACS. Covalent organic frameworks: a materials platform for structural and functional designs. 2016;138(33):10104-10119.
76. Huang Y-B, Liang J, Wang X-S, Cao RJC. Multifunctional metal–organic framework catalysts: synergistic catalysis and tandem reactions. 2017;23(33):16498-16523.
77. Huang Y-B, Qin J-S, Jiang H-L, Zhou H-CJMC. Covalent organic frameworks for catalysis. 2016;24(42):7396-7404.
78. Huo J, Aguilera-Sigalat J, El-Hankari S, Bradshaw DJMC. Magnetic metal–organic frameworks for potential imaging and drug delivery. 2015;21(19):7369-7373.
79. Huxford RC, Della Rocca J, Lin WJCCR. Metal–organic frameworks as potential drug carriers. 2012;111(12):7523-7546.
80. Janiak CJCCR. Engineering coordination polymers towards applications. 2003;236(1-2):23-47.
81. Ji Z, Wang H, Canossa S, Wuttke S, Yaghi OMJAS. Pore chemistry of metal–organic frameworks. 2020;367(6476):795-800.
82. Jiang H-L, Feng D, Liu T-F, Li J-R, Zhou H-CJACIE. Pore surface engineering with controlled loadings of functional groups via click chemistry in highly stable metal–organic frameworks. 2012;51(4):1007-1010.
83. Jiang H-L, Liu B, Akita T, Haruta M, Sakurai H, Xu QJACS. Au@ ZIF-8: CO oxidation over gold nanoparticles deposited to metal–organic framework. 2009;131(32):11302-11303.
84. Jiang H-L, Makal TA, Zhou H-CCCS. Interpenetration control in metal–organic frameworks for functional applications. 2013;4(4):567-579.
85. Jiang H-L, Xu QJCS. Porous metal–organic frameworks as platforms for functional applications. 2011;2(3):480-493.
86. Jiang J, Yaghi OMJACS. Brønsted acidity in metal–organic frameworks. 2015;137(41):13706-13709.
87. Johnson JA, Zhang X, Reeson TC, Chen Y-S, Zhang JJM. Isoreticular metal–organic frameworks with tetrahedral building blocks and octahedral metal–oxide clusters. 2012;134(20):7317-7320.
88. Kalmutzki MJ, Diercks CS, Yaghi OMAM. Metal–organic frameworks for water harvesting from air. 2018;30(23):1704304.
89. Kandiah M, Nilsen MH, Usseglio S, Jakobsen S, Olsbye U, Tilset M, Larabi C, Quadrelli EA, Bonino F, Lillerud KPJMC. Synthesis and stability of tagged UiO-66 Zr-MOFs. 2010;22(33):6632-6640.
90. Kang Y, Wang F, Zhang J, Wang Z, Wang G, Chen H, Wu T, Bu X, Feng PJC. A multivariate MOF as a superior catalyst for oxidative desulfurization. 2015;21(46):17650-17657.
91. Karagiaridi O, Bury W, Mondloch JE, Hupp JT, Farha OKACIE. Solvent-assisted linker exchange: an alternative to the de novo synthesis of metal–organic frameworks. 2014;53(18):4530-4540.
92. Karagiaridi O, Lalonde MB, Bury W, Sarjeant AA, Farha OK, Hupp JTJACS. Opening ZIF-8: a catalytically active zeolitic imidazolate framework of sodalite topology with unsubstituted linkers. 2012;134(45):18790-18796.

93. Katz MJ, Brown ZJ, Colón YJ, Siu PW, Scheidt KA, Snurr RQ, Hupp JT, Farha OKCJ. A facile synthesis of UiO-66, UiO-67 and their derivatives. 2013;19(14):4305-4314.
94. Kaye SS, Long JRJACS. Hydrogen storage in the dehydrated Prussian blue analogues M3 [Co (CN) 6] 2 (M= Mn, Fe, Co, Ni, Cu, Zn). 2005;127(18):6506-6507.
95. Kreno LE, Leong K, Farha OK, Allendorf M, Van Duyne RP, Hupp JTCCR. Metal–organic framework materials as chemical sensors. 2012;112(2):1105-1125.
96. Kuppler RJ, Timmons DJ, Fang Q-R, Li J-R, Makal TA, Young MD, Yuan D, Zhao D, Zhuang W, Zhou H-CCCR. Potential applications of metal–organic frameworks. 2009;112(2):724-781.
97. Kutzscher C, Hauser J, Nickerl G, Senkovska I, Kaskel SJMC. Luminescent MOF films and membranes for chemical sensing. 2016;24(18):3824-3830.
98. Lan A, Li K, Wu H, Olson DH, Emge TJ, Ki W, Hong M, Li JPNAS. A luminescent microporous metal–organic framework for the fast and reversible detection of high explosives. 2009;106(23):8656-8661.
99. Lee J, Farha OK, Roberts J, Scheidt KA, Nguyen ST, Hupp JTCR. Metal–organic framework materials as catalysts. 2009;109(9):552-622.
100. Lee Y-R, Kim J, Ahn WSCR. Synthesis of metal–organic frameworks: a mini review. 2017;46(1):145-160.